ASTRONOMY & ASTROPHYSICS
SUPPLEMENT SERIES

Astron. Astrophys. Suppl. Ser. **103,** 245-271 (1994)

Multicolor photometry of clusters of galaxies: A3284, A3305, A1942*,**

E. Molinari[1], M. Banzi[1], A. Buzzoni[1], G. Chincarini[1,2] and M.D. Pedrana[1]

[1] Osservatorio Astronomico di Brera, Via Brera, 28 20121 Milano, Italy
[2] Dip. di Fisica dell'Università degli Studi, Via Celoria, 16 20133 Milano, Italy

Received May 11; accepted June 25, 1993

Abstract. — We present complete multicolor photometry in the Gunn system for the three clusters of galaxies A3284, A3305 and A1942 at redshift $z \sim 0.2$. INVENTORY magnitudes and colours have been obtained for over 1,000 objects in the three fields down to $g = 24$, and with a good completeness level in the detections (85% or better) about one magnitude brighter. By fitting with King profiles the r counts we derived the total number of galaxies and the core radius down to the r magnitude limit in each cluster. These are $N_{TOT} = 146$ galaxies and $R_c = 0.24$ Mpc for A3284, $N_{TOT} = 129$ and $R_c = 0.20$ Mpc for A3305, $N_{TOT} = 130$ and $R_c = 0.24$ Mpc for A1942. The observed mean redshift of the clusters is $z = 0.150 \pm 0.001$ for A3284, $z = 0.157 \pm 0.001$ for A3305, and $z = 0.226 \pm 0.001$ for A1942. The $c-m$ diagrams and the $g-i$ colour distribution as well as the two-colour diagrams are used to single out early-type galaxies and spirals on the basis of their different photometric properties. This approach aimed at a self-consistent classification of galaxies on the basis of photometric indicators will be further developed for a systematic study of the galaxy population in distant clusters.

Key words: galaxies: clustering — galaxies: clusters: individual: A1942, A3284, A3305 — galaxies: evolution — galaxies: photometry

1. Introduction

To a very large extent the understanding of cosmology is related to the observation of distant faint galaxies. This holds especially if we want to study how galaxies evolve with time as it seems clear that, at some point early in the primeval evolution, phenomena related to the environment must have had a profound influence in what happened.

Butcher & Oemler (1978) first noticed that in two clusters at redshift $z > 0.4$ the overall population of galaxies looked remarkably different compared with similar low-redshift clusters. In particular, an excess of blue galaxies seemed to appear at large look-back times. Among others, also Dressler & Gunn (1982) using spectroscopy and [OII] photometry confirmed this scenario arguing that evolutionary effects could already have been at hand at those distances.

To date, there is a general consensus about the existence of the Butcher-Oemler effect (Newberry et al. 1988; Luppino et al. 1991; Dressler & Gunn 1992) but still large observational and statistical uncertainties do not allow a precise quantification of the phenomenon and of the physical mechanisms at work. For example, evolutionary models predict that star formation could have proceeded more effectively some Gyr ago in late-type galaxies (Sandage 1986; Ferrini & Galli 1988), and this could be in the sense of enhancing the blue galaxy population in the past as also recent high-resolution observations with HST of clusters at $z \sim 0.4$ seem to suggest (Dressler 1993). However, whatever be the primary mechanisms causing the blue excess, it remains to be firmly established whether they are still at work at the present time or rather appear abruptly beyond $z \sim 0.1$.

Most of the studies searching for evolutionary effects in distant galaxies deal with clusters. The rationale is rather evident: if we observe a homogeneous set of objects all at the same distance it might be reasonable to assume them to be also coeval so that we can retrieve more confidently their intrinsic environmental static and dynamical characteristics. A common limitation to this approach is that cluster selection based on optical catalogs introduces

Send offprint requests to: Emilio Molinari Osservatorio Astronomico di Brera, Via E. Bianchi, 46 22055 Merate, Italy

* Based on observations made at the European Southern Observatory (ESO) La Silla, Chile

** Tables 3, 4 and 5 are also available in electronic form at the CDS

strong biases against the selection of the most distant aggregates (Koo 1988; Cappi et al. 1989; Philipps et al. 1990) including spurious optical projections as false candidates (see for example Ellis et al. 1985 for the case of 0016+16). Some of these uncertainties could be partially recovered using X-ray selected samples as for example the Einstein medium-sensitivity survey (Stocke et al. 1991) or the ROSAT sky survey (Trumper 1991).

Since 1986 we started a systematic survey of clusters of galaxies (mainly optically selected) at intermediate and large redshift. Through comparison with evolutionary population synthesis models (Buzzoni 1989) we intend to check how consistently do photometric properties of galaxies in cluster evolve in a quiescent way, i.e. following the prescription of stellar evolution. All those which deviate from the expectations will tell us something new, that is about events which have perturbed and/or accelerated the normal course of evolution. A general approach to the problem has been outlined in the previous contributions to this project that can be found in Buzzoni et al. (1988); Molinari et al. (1990, hereafter MBC90); Molinari et al. (1992); Buzzoni et al. (1992); Molinari (1993).

In this work, the first of two accompanying papers, we present the observations for three clusters at intermediate redshift ($z \sim 0.2$) selected from the revised Abell catalog (Abell et al. 1989). They are A3284, A3305 and A1942, and Table 1 summarizes their relevant parameters. High-resolution NTT observations of a more distant set ($z \sim 0.5$) will be then the subject of a third paper that will address more extensively the problem of the environmental and evolutionary status of cluster galaxies. Spectroscopic observations will also be presented and discussed separately.

The paper is arranged with Sect. 2 reporting on observations and data reduction. The complete photometric catalogs of the objects in the fields are given in Sect. 3 while Sect. 4 shows the first steps to the data analysis.

2. Data acquisition and calibration

2.1. The data

Observations have been carried out at the 3.6 m ESO telescope at La Silla (Chile). The CCD frames have been obtained using EFOSC (ESO faint objects spectrograph and camera) during three observing runs between 1986-90. In Tables 2a, b, c we report a detailed log of the observations. During the first run in November 1986 the EFOSC images were affected by scattered light. This was due to a poor design of the window of the dewar which caused a "donut"-shaped excess of scattered light near the centre of the field at a level of about 5–10% over the sky background. We devised a procedure to correct for it and however the photometric accuracy was somewhat degraded (see MBC90 for details). The design of the dewar's windows was modified in 1987 so that the two supplementary runs in November 1987 and April 1990 were of higher photometric quality. Images were obtained in the Gunn g, r and i system as defined in Thuan & Gunn (1976) and Wade et al. (1979). The efficiency of the system CCD + filter + detector is at most about 40%. Details of the response of EFOSC and RCA CCD #8 detector are given in MBC90 and Molinari (1993) while the use of RCA CCD #11 (since 1990) did not yield any relevant difference in reproducing the standard photometric system.

We were not favored by excellent atmospheric conditions. The seeing disk was typically about 1.5 arcsec FWHM and this limited resolution in crowded fields restoring blended images. In addition, the effective FWHM slightly degraded to the values reported in Table 2 after re-coordinating and stacking the original frames. This has not affected however the possibility of cross-correlating the positions in the images corresponding to the three colours.

The 640×1032 15 μm pixel CCD #8 and #11 were used in the binned mode supplying an effective 30 μm element resolution with an angular scale of 0.675 arcsec per binned pixel. The useful field of view was about 3.2×5.3 arcmin.

2.2. Redshift determination

In addition to imaging, spectra were taken in order to determine the redshift including a total of 23 member galaxies in the three clusters. All the observations have been carried out using EFOSC in multi-object spectroscopy (MOS) mode. The dispersion was 230 Å/mm with a FWHM resolution of 14.5 Å at 5000 Å. Our estimates of the mean redshift of the clusters together with their 1σ statistical uncertainties are included in Table 1.

Spectroscopic observations for the cluster A1942 are also available from Leir & van den Bergh (1977), who found $z = 0.209$, and from Kristian et al. (1978) ($z = 0.224$). Furthermore, photometry on this cluster has been carried out by Couch et al. (1983), and Couch & Newell (1984). Our spectroscopic observations support the redshift estimate by Kristian et al. (1978). Assuming (H_o, q_o) =(50 km/s/Mpc, 0) throughout the paper, this leads to a look-back time of 2.5, 2.6 and 3.6 Gyr for A3284, A3305 and A1942, respectively.

2.3. Image processing

Data reduction was performed using the MIDAS software package produced at ESO (see MIDAS Users Guide, Image Processing Group ESO V4.3 1988) running both on VMS and UNIX computers at the Brera Astronomical Observatory. Because of the problems with the scattered light mentioned above, in addition to the usual flat-fielding and cleaning procedures we had to model the pattern of

the spurious light. This has been done by means of the dome flat-fields. The properly rescaled template pattern was then subtracted from every image, and only after this we used the twilight flat-fields to remove the high spatial frequencies in the CCD response while the dome flat-fields were used for recovering the low frequencies (see MBC90 and Molinari 1993 for a full description of the reduction procedure).

Image reduction was more straightforward for the observations carried out after 1987. In this case the flat-field derived from the scientific frames by shifting for some pixel each partial exposure and computing then the median frame. The overall cleaning procedure led to a low rms scatter in the sky background always less than 1% of the sky signal (cf. Table 2).

2.4. *Photometric calibrations*

The 1986 and 1987 observations were calibrated using Landolt (1973) standard stars. As magnitudes were available only in the Johnson system a transformation to the Gunn system was necessary through appropriate colour equations derived from the Vilnius spectral atlas of stars (Straižys & Sviderskiene 1972). As discussed in MBC90, the transformation procedure yielded a 1σ uncertainty of 0.02 mag in the g and r magnitudes, and a larger 0.04 mag for the i band. Primary Gunn's standards, namely Wolf 437, Ross 453, and Ross 484, were used on the contrary in the other runs.

Magnitude variations in the photometry repeated on different frames can be mainly ascribed to Poisson statistical fluctuations so that the expected uncertainty scales as $10^{0.2\ \mathrm{mag}}$. As an example, this is shown in Fig. 1 for the A3284 photometry (two frames are available in the r band at 900 s and 300 s exposure time, cf. Table 2a). Plotted in the figure are the magnitude differences for each of the objects detected in the 900 s frame with respect to the time-weighted mean magnitude from the two frames defined as $\bar{m} = (9m_{900} + 3m_{300})/12$.

With little arithmetic, one can derive

$$m_{900} - \bar{m} = \frac{m_{900} - m_{300}}{4}. \qquad (1)$$

As the Poisson variance of magnitudes scales linearly with the exposure time, the statistical variance of the points in Fig. 1 can be written as

$$\sigma = \frac{\sigma_{900}^2 + 3\sigma_{900}^2}{4} = \frac{4}{3}\sigma_{1200} \qquad (2)$$

from which it is immediate to derive the variance σ_{1200} expected for the 1200 sec coadded frame. The errors quoted in Table 2 are comprehensive of all the uncertainties caused by the photon statistics, transformation equation between photometric systems and offset errors due to standard stars. All errors have been square coadded, and refer typically to objects about magnitude 22.

As it can be seen in Table 2, the data for A1942 and the i observations for A3284 are of inferior quality mainly due to the poor sky conditions which added some uncertain systematic fluctuation.

3. The catalogs

Recognition and systematic photometry of the objects in the fields was derived using the INVENTORY package (West & Kruszewski 1981; Kruszewski 1989) implemented in the MIDAS environment. Basically, we searched for all objects exceeding a 1% threshold over the local sky background. As a consequence, the isophotal magnitudes are at different levels in each filter, i.e. about five magnitudes fainter than the sky brightness reported in Table 2.

Colours were obtained instead over fixed apertures with a 4 or 6 pixel diameter retaining the largest one still compatible with the isophotal radius in the r band. When the case, the elliptical shape of the objects has been automatically accounted for by INVENTORY in the photometry. However, it is clear from Fig. 2 that fainter than $r \sim 20$ any morphological feature has been erased and we are essentially dealing with seeing-limited objects. For all clusters we reached a magnitude limit about $g \sim 24$ with a good completeness level (85% or better) in the object detection about one magnitude brighter (see Fig. 3).

The photometric catalogs for A3284, A3305 and A1942 are presented in Tables 3, 4, and 5. A total of 455 objects have been measured in the field of A3284, 281 in the field of A3305, and 270 in A1942. For these, about 50% (486 objects in total) have complete g, r, i photometry. In the tables, for each object Col. (1) lists an identification number, while Cols. (2) and (3) give the relative coordinates in pixels on the frames (1 px=0.675 arcsec.) The next three Cols. (4, 5, 6) in the catalogs are the isophotal magnitudes, while aperture colours g-r and g-i are reported in Cols. (7) and (8). Finally, in Col. (9) we list the isophotal radius (in pixels) used for the r magnitude when available. Note that some bright stars (about five in each field with $r \leq 16$) saturated on the frames have not been included in the catalogs.

The origin of the coordinates in the tables is set at the adopted centre of the clusters defined by making a count number histogram of all objects projected on the X and Y axes and fitting then each distribution with a Gaussian curve. This centre does not necessarily correspond to the nominal coordinates of Table 1 taken directly from Abell et al. (1989).

Images of the three clusters in the r band are reproduced in panels a of Figs. 4, 5, and 6 faced to their cross identification charts in panels b. Smoothed density maps

for each cluster using the whole entries in the photometric catalogs are also displayed in Fig. 7 to give an indication of the overall morphology.

By fitting with a King profile the r sample in each count density map we evaluated the total number of member galaxies down to the r magnitude limit, and the core radius of the clusters. A3284 results the richest cluster with a total of $N_{\rm TOT} = 146$ galaxies and a core radius $R_{\rm c} = 0.24$ Mpc. In this case however a cD galaxy clearly dominates the field probably affecting the counts and the apparent morphology of the cluster. Due to its relevance, for this galaxy (it is object no. 455 in Table 3) we give only the estimated total magnitudes deferring a more detailed study of its surface brightness and spectral properties to a separate note (Molinari et al. 1993). Finally, for A3305 we have $N_{\rm TOT} = 129$ galaxies and $R_{\rm c} = 0.20$ Mpc, while A1942 contains 130 galaxies with $R_{\rm c} = 0.24$ Mpc. A χ^2 test operated on the fit algorithm allowed to derive a ± 0.005 Mpc error bar for the inferred $R_{\rm c}$ while a $\pm 8\%$ uncertainty affects the estimated $N_{\rm TOT}$, both error bars referring to a 90% confidence level. The observed spatial distribution of the clusters compared with the fitting King profiles is displayed in Fig. 8.

From the figure it is also interesting to note the different levels of the background according to the different magnitude limits in Table 2. A change from $r_{\rm lim} = 22.5$ to $r_{\rm lim} = 24.5$ increases the counts by a factor of 3.5. As a reference value, at $r_{\rm lim} = 23.5$ we find about 3 10^4 obj/deg^2 in agreement also with the observations in MBC90.

4. Data analysis

4.1. *Colour distribution and colour-magnitude diagrams*

In Fig. 9 we show the colour distribution for the whole sample of objects in the field of each cluster. The more striking feature in all of the three plots is a prominent peak of red objects about $g - i \simeq 1$. According also to Dixon et al. (1989); MBC90; Luppino et al. (1991); Molinari et al. (1992) we are inclined to identify these red objects with a population of fiducial early-type galaxies. It is undoubtedly true of course that at such large distances we are not able to check directly our assumption but, on the other hand, we have nothing against this hypothesis, and moreover it is fair to notice that the colours measured in distant cluster galaxies are essentially consistent with those of present-day homologues, after proper k-correction (Newberry et al. 1988; Pickles & Van der Kruit 1991; Dressler & Gunn 1992). Furthermore, this assumption is in agreement with the spectra we collected for each cluster.

A smaller and bluer peak containing the Butcher-Oemler galaxies is visible in the colour distribution of Fig. 9 especially for A3284. Once accounted for the differential k-correction, this feature is very similar to what found for Cl2158+0351, at $z = 0.45$ (MBC90). On the basis of the apparent colours expected at the relevant redshift we attribute this blue bump to spiral galaxies. The bump apparently disappears in A3305 and A1942, although from the colour distributions there are hints for a blue excess. For A1942 this is partly due to a larger photometric error that contributes in blurring the colour distribution.

The wing of the distribution toward even bluer colours ($g - i \sim 0$) is due to Galactic F-G stars, and foreground galaxies of different morphological types (cf. Fig. 13 in MBC90), while the extreme red wing is populated on the contrary by a few M dwarf star (about $g - i \sim 1.5$) and by galaxies in the background.

The overall features of the galaxy population in the clusters are even more evident in the $c-m$ diagram of Fig. 10. Again, early-type galaxies clearly appear lying along a nearly vertical strip, and especially for A3284 one can appreciate the Visvanathan-Sandage (1977) effect with the brightest ellipticals to be also the reddest ones. Quite interestingly, also the cD galaxy fits the same relationship.

The blue bump seen in Fig. 9 for this cluster can be easily recognized here as an excess of objects fainter than $r \sim 23$. Indeed, we might conclude that a huge number of intrinsically faint spirals seems to populate the cluster, a feature that closely resembles that observed for Cl 2158+0351 (MBC90). In addition to our previous discussion, it is worth noting by inspection of Fig. 10 that the apparent lack of a prominent blue bump in the galaxy population of A3305 and A1942 might reside in the less deep photometry.

4.2. *The two-colour plane*

The $(g - r)/(g - i)$ plots for the clusters are reproduced in Fig. 11. As stated above, in each of this plot it is easily recognized the higher density clump which define the locus of red (alias elliptical) galaxies. On the top right panel we have also reproduced the theoretical loci expected for galaxies of different morphological types with increasing redshift. The path in the $(g-r)/(g-i)$ diagram has been obtained by convolving the mean spectral energy distribution of selected templates with the relevant photometric system. Sources of reference spectra are Coleman et al. (1980) and Pence (1976) for spirals while ellipticals come from theoretical models for evolutionary population synthesis by Buzzoni (1989) assuming a burst stellar population with a Salpeter IMF and [Fe/H] = +0.20 according to Buzzoni et al. (1992).

Expected evolutionary path in the $(g - r)/(g - i)$ diagram matches well the observed distribution of the cluster galaxies. As we anticipated in previous section, it also appears that only distant ($z \geq 0.5$) early-type galaxies are able to venture to extremely red apparent colours dominating the population of objects beyond $g-i \geq 2.0$. In this sense, a reliable detection of the locus of cluster early-type

galaxies in two-colour or $c-m$ diagrams can pose a confident constraint to the discrimination of distant galaxies in the background.

The pretty good agreement between observations and theoretical expectations leads us to conclude that at least up to $z \sim 0.2$ the overall photometric properties of the galaxies do not show any evident sign of peculiarity. In particular, we can state that no direct evidence is found for pervasive ongoing star formation affecting the early-type galaxy component in the cluster population. This could be an encouraging point for using cluster elliptical galaxies as reliable standard candles (Buzzoni et al. 1993).

Acknowledgements. We would like to acknowledge referee's careful review of the original version of the paper that greatly contributed improving the data presentation and the general discussion. Thanks are for Mr. S. Cantù at OAB for his valuable help in the technical set up of the figures and tables.

References

Abell G.O., Corwin H.G. Jr, Olowin R.P. 1989, ApJS 70, 1
Burstein D., Heiles C. 1982, AJ 87, 1165
Butcher H., Oemler A. 1978, ApJ 219, 18
Buzzoni A. 1989, ApJS 71, 817
Buzzoni A., Gariboldi G., Mantegazza L. 1992, AJ 103, 1814
Buzzoni A., Chincarini G., Molinari E. 1993, ApJ 410, 499
Buzzoni A., Molinari E.C., Manousoyannaki I., Chincarini G. 1988, The ESO Messenger 53, 50
Cappi A., Chincarini G., Conconi P., Vettolani G. 1989, A&A 223, 1
Coleman G.D., Wu C., Weedman D.W. 1980, ApJS 43, 393
Couch W.J., Newell E.B. 1984, ApJS 56, 143
Couch W.J., Ellis R.S., Godwin J., Carter D. 1983, MNRAS 205, 1287
Dixon K.L., Godwin J.G., Peach J.V. 1989, MNRAS 239, 459
Dressler A. 1980, ApJ 236, 351
Dressler A. 1993, in: Observational Cosmology, eds. G. Chincarini, T. Maccacaro, A. Iovino, D. Maccagni, ASP Conf. Ser., 225
Dressler A., Gunn J.E. 1982, ApJ 263, 533
Dressler A., Gunn J.E. 1992, ApJS 76, 813
Ellis R.S., Couch W.J., MacLaren I., Koo D.C. 1985, MNRAS 217, 239
Ferrini F., Galli D. 1988, A&A 195, 27
Koo D.C. 1988, in: Erice Workshop, Towards Understanding Galaxies at Large Redshift, eds. R.G. Kron and A. Renzini (Dordrecht, Kluwer) 275
Kruszewski A. 1989, in the First ESO/ST-ECF, Data Analysis Workshop, eds. P.J. Grosbol, F. Murtagh and R.H. Warwels (Garching, ESO) 29
Kristian J., Sandage A., Westphal J.A. 1978, ApJ 221, 383
Landolt A.U. 1973, AJ 78, 959
Leir A.A., van den Bergh S. 1977, ApJS 34, 381
Luppino G.A., Cooke B.A., McHardy I.M., Ricker G.R. 1991, AJ 102, 1
Molinari E. 1993, Ph.D. Thesis dissertation (Univ. of Milano)
Molinari E., Buzzoni A., Chincarini G. 1990, MNRAS 246, 576 (MBC90)
Molinari E., Pedrana M.D., Banzi M., Buzzoni A., Chincarini G. 1992, in: proceedings of the IAU Symp. no. 149 The Stellar Populations of Galaxies, eds. B. Barbuy and A. Renzini (Dordrecht, Kluwer) in press
Molinari E., Buzzoni A., Chincarini G., Pedrana M.D. 1993, in preparation
Newberry M.V., Kirshner R.P., Boroson T.A. 1988, ApJ 335, 629
Pence W. 1976, ApJ 203, 39
Phillipps S., Davies J.I., Disney M.J. 1990, MNRAS 242, 235
Pickles A.J., van der Kruit P.C. 1991, ApJS 91, 1
Sandage A. 1986, A&A 161, 89
Stocke J.T., Morris S., Gioia I., Maccacaro T., Schild R., Wolter A., Fleming T.A., Henry J.P. 1991, ApJS 76, 813
Straižys V., Sviderskiene Z. 1972, Bull. Vilnius Astr. Obs. 35, 1
Thuan T.X., Gunn J.E. 1976, PASP 88, 543
Trumper J.E. 1991, in: Schloss Ringberg Workshop, Traces of the Primordial Universe, eds. H. Böhringer and R.A. Treumann (Garching bei München, MPE Report 227) 163
Visvanathan N., Sandage A. 1977, ApJ 216, 214
Wade R.A., Hoessel J.G., Elias J.H., Huchra J.P. 1979, PASP 91, 35
West R.M., Kruszewski A. 1981, Irish Astron. J. 15, 25

Table 1. Relevant clusters parameters

Name	Coord. (1950) α	δ	l	b	z	m-M	T_{BM}	RC	DC	E_{B-V}
A3284	$04^h39.8^m$	$-45°09'$	250.3	−41.2	0.150±0.001	39.9	I	1	6	0.00
A3305	$05^h00.2^m$	$-39°17'$	242.5	−36.9	0.157±0.001	40.0	I-II	2	5	0.00
A1942	$14^h36.1^m$	$+03°53'$	355.4	+54.8	0.226±0.001	40.9	III	3	6	0.02

Notes to the table:
$m - M = 5log\ d_L + 25$ with d_L the luminosity distance in Mpc from z with the adopted cosmology; T_{BM}: Bautz-Morgan class; RC: richness class from ACO catalog;
DC: distance class from ACO catalog; E_{B-V}: colour excess from Burstein and Heiles (1982).

Table 2a. Observations log for A3284

filter	date	CCD#	exp time (sec)	airmass
g	1986 Nov 4	# 8	1200	1.049
r	1986 Nov 4	# 8	900	1.042
r	1986 Nov 4	# 8	300	1.044
i	1987 Nov 20	# 11	600	1.126
i	1987 Nov 20	# 11	600	1.149
i	1987 Nov 21	# 11	600	1.240

Characteristics of the coadded images

filter	exp time (sec)	mag lim	obj (no.)	mag err	sky bright. (mag arcsec^{-2})	sky rms	PSF (arcsec)
g	1200	25.0	324	0.08	21.72	0.9%	2.1
r	1200	24.5	384	0.08	21.66	0.6%	2.0
i	1800	24.0	243	0.28	21.27	0.4%	1.9

455 objects detected. 203 with complete *g*, *r*, *i* photometry.

Table 2b. Observations log for A3305

filter	date	CCD#	exp time (sec)	airmass
g	1986 Nov 4	# 8	900	1.021
r	1986 Nov 4	# 8	600	1.028
i	1986 Nov 4	# 8	1200	1.042

Characteristics of the coadded images

filter	exp time (sec)	mag lim	obj (no.)	mag err	sky bright. (mag arcsec^{-2})	sky rms	PSF (arcsec)
g	900	24.5	237	0.08	21.66	0.9%	2.2
r	600	22.5	161	0.08	21.01	1.0%	2.1
i	1200	22.5	163	0.08	20.46	0.8%	2.4

281 objects detected. 123 with complete *g*, *r*, *i* photometry.

Table 2c. Observations log for A1942

filter	date	CCD#	exp time (sec)	airmass
g	1990 Apr 18	# 11	600	1.273
g	1990 Apr 18	# 11	600	1.472
g	1990 Apr 18	# 11	600	1.534
r	1990 Apr 18	# 11	600	1.300
r	1990 Apr 18	# 11	600	1.420
r	1990 Apr 18	# 11	600	1.605
i	1990 Apr 18	# 11	600	1.333
i	1990 Apr 18	# 11	600	1.375
i	1990 Apr 18	# 11	600	1.686

Characteristics of the coadded images

filter	exp time (sec)	mag lim	obj (no.)	mag err	sky bright. (mag arcsec^{-2})	sky rms	PSF (arcsec)
g	1800	24.0	201	0.26	20.75	0.4%	2.4
r	1800	23.5	229	0.24	20.40	0.3%	2.5
i	1800	23.0	204	0.27	19.65	0.3%	2.7

270 objects detected. 160 with complete *g*, *r*, *i* photometry.

Table 3. Catalog of the cluster A3284

No.	X_{pix}	Y_{pix}	g	r	i	g-r	g-i	R_{iso}
1	139.6	-262.9	24.98					
2	44.9	-262.2	24.89					
3	150.5	-261.8	19.07		17.66		1.60	
4	-1.3	-258.2	21.31	21.17	20.90	0.18	0.47	3.70
5	97.6	-256.4	24.40	24.27		0.07		1.60
6	-42.3	-253.7	22.74	21.43	20.44	1.22	2.20	3.70
7	164.0	-253.6	23.01	21.96	21.90	0.95	1.05	3.50
8	113.1	-249.0		24.71				1.20
9	146.9	-248.6	19.57	19.22	18.90	0.32	0.64	8.80
10	105.4	-246.6	20.37	19.72	19.33	0.63	1.01	7.60
11	92.5	-245.4	24.36	25.01		-0.52		1.00
12	98.9	-244.4	24.84					
13	187.3	-243.3		24.36				1.60
14	82.8	-243.2		24.28				1.70
15	-33.9	-242.8	22.84	22.62	22.37	0.19	0.49	3.20
16	-66.5	-242.2	25.28					
17	142.5	-242.2	23.04	22.28		0.65		3.80
18	161.4	-241.4		24.02				1.80
19	-20.8	-241.1	24.57	24.50		0.15		1.40
20	-43.7	-240.9	23.69	23.06	23.06	0.59	0.56	2.50
21	-62.2	-239.2		25.06				1.10
22	80.7	-237.1	24.18	23.49	22.91	0.56	1.16	2.00
23	-82.7	-232.1	22.32	21.71	21.07	0.60	1.11	3.70
24	-65.9	-230.4			16.22			
25	-7.3	-230.2	23.94	23.60	23.33	0.40	0.81	2.10
26	12.7	-229.8			16.51			
27	55.8	-229.1	22.93	22.27	22.10	0.58	0.83	3.60
28	93.7	-228.5	24.37	23.03	21.59	1.17	2.55	2.20
29	134.2	-228.5	23.60	23.05	22.82	0.27	0.68	2.80
30	-27.5	-226.6	23.58	23.83	23.64	-0.26	0.15	2.10
31	115.6	-226.6	21.57	20.85	20.42	0.71	1.16	4.60
32	116.5	-221.7		24.59				1.30
33	-73.2	-221.2		23.32				2.60
34	103.5	-219.5	24.49					
35	-61.2	-216.9		23.49				2.30
36	150.2	-214.9		25.22				0.90
37	199.9	-214.5		22.29				3.80
38	165.9	-213.2		25.20				0.90
39	179.0	-212.5	23.12	21.45		1.45		4.60
40	-65.4	-211.3	22.99	21.84	20.80	1.10	2.07	3.40

No.	X_{pix}	Y_{pix}	g	r	i	g-r	g-i	R_{iso}
41	-90.3	-209.8	24.51	23.74	23.24	0.67	1.03	1.80
42	58.4	-209.7			24.00			
43	68.1	-209.7	23.64	23.55	23.43	-0.08	0.28	2.20
44	91.8	-209.2	25.12	24.12		0.62		1.70
45	52.1	-209.1	24.10	23.56	22.75	0.49	0.95	1.90
46	139.8	-208.4		24.31				1.60
47	99.3	-205.7	20.96	20.33	20.02	0.67	1.02	5.30
48	203.6	-203.2		22.11				4.00
49	14.4	-201.8		25.09				1.00
50	179.8	-201.4	25.19					
51	58.7	-201.3	23.54	23.40	22.66	0.38	0.88	2.00
52	131.5	-200.9	24.80					
53	-31.3	-200.5	25.02					
54	-54.9	-200.2		24.78				1.20
55	83.0	-196.2			23.02			
56	-76.1	-194.6		25.21				0.90
57	195.2	-188.5	23.13	22.69		0.55		2.50
58	154.6	-186.6	21.65	21.05	20.76	0.63	0.98	4.40
59	60.6	-185.9	25.07	24.61		0.34		1.30
60	53.6	-185.8		23.98				1.90
61	-89.9	-183.3	22.47	22.18	22.13	0.31	0.45	3.30
62	-1.5	-181.9	24.96	24.30		0.37		1.60
63	107.8	-178.6	25.10	24.24		0.77		1.50
64	8.3	-176.6	20.42	19.73	19.28	0.70	1.15	5.60
65	81.9	-174.7	20.66	19.46	18.35	1.22	2.34	5.40
66	31.8	-174.5			16.47			
67	160.5	-174.4	23.70	23.23	23.18	0.39	0.56	2.70
68	-72.6	-173.9	23.73	22.90	22.96	0.55	0.72	3.30
69	-42.2	-171.2	22.00	21.27	20.76	0.65	1.14	4.40
70	189.5	-170.8	22.56	23.11		-0.22		2.50
71	-57.2	-170.4		24.58				1.40
72	-31.0	-170.2		24.92				1.00
73	94.2	-165.5	23.35	23.28	22.31	0.09	0.85	2.50
74	174.3	-164.9	24.31	23.73	23.19	0.43	0.64	1.70
75	63.3	-162.6	24.53	24.10		0.32		1.70
76	-36.1	-161.1		18.24	18.05			6.90
77	-87.4	-160.4		24.78				1.20
78	13.3	-159.7	25.25					
79	-1.6	-159.5	25.13	23.51		0.99		2.30
80	81.6	-158.1		24.53				1.40

Table 3. continued

No.	X_{pix}	Y_{pix}	g	r	i	g-r	g-i	R_{iso}
81	119.6	-156.4	19.76	18.51	17.44	1.25	2.34	7.30
82	-31.4	-154.2		22.65				2.50
83	-55.8	-152.5	23.12	22.78	22.31	0.51	1.01	2.60
84	-94.2	-152.0	20.67	19.50	18.59	1.16	2.06	5.50
85	-64.4	-150.4	20.05	20.04	19.68	0.12	0.40	5.30
86	147.4	-150.0	23.33	22.05	20.94	1.15	2.23	3.20
87	81.8	-149.1	24.35	23.68	23.78	0.42	0.58	2.10
88	183.8	-149.1	25.22					
89	44.2	-148.2		25.20				0.90
90	-5.5	-143.0	23.83		23.62		0.53	
91	151.0	-140.4	24.92					
92	130.8	-138.7	22.21	21.81	21.88	0.43	0.44	3.70
93	-47.1	-136.2	19.47	18.76	18.42	0.67	1.05	11.50
94	-73.9	-133.7		21.61				4.30
95	99.4	-129.8	25.27					
96	-8.0	-128.6	22.54	21.98	21.80	0.60	0.82	3.20
97	-28.5	-128.0		24.83				1.00
98	169.9	-127.8	25.02					
99	141.5	-127.8	23.53	23.30	22.51	0.40	1.04	2.00
100	84.4	-127.4	23.61	23.51	22.75	0.10	0.96	2.30
101	59.2	-127.3		24.66				1.30
102	111.2	-125.2	20.89	20.65	20.43	0.25	0.52	4.70
103	18.6	-124.6	20.39	19.15	17.96	1.32	2.49	5.80
104	53.1	-123.2		25.19				0.90
105	129.0	-122.8	22.83	22.16	21.62	0.65	1.12	3.20
106	182.3	-122.3	20.22	20.11		0.14		4.80
107	4.9	-122.0	22.66	22.05	21.71	0.60	0.95	3.40
108	-6.7	-121.3	25.09					
109	86.7	-118.5	24.58		23.16		1.10	
110	-0.3	-117.8	23.50	22.64	22.27	0.82	0.96	2.80
111	128.7	-114.2		24.51	22.74			1.30
112	43.7	-111.8	22.17	22.22	21.95	-0.05	0.27	3.00
113	205.6	-106.7		22.33				3.40
114	66.5	-106.5	20.94	20.80	20.61	0.17	0.40	5.40
115	172.6	-106.4	23.29	23.21	23.17	0.02	0.32	2.80
116	-2.6	-105.6	24.27					
117	183.3	-104.9	21.92	21.34		0.62		4.20
118	-97.6	-101.8	24.65	24.65		-0.08		1.40
119	-8.6	-100.9	21.80	21.05	20.91	0.68	0.99	4.90
120	91.0	-100.4		24.75				1.10
121	-89.4	-100.3		25.09				0.90
122	113.9	-98.4	24.15	24.02	23.75	-0.04	0.47	1.90
123	-58.0	-97.8	21.53	21.55	21.35	0.06	0.29	3.90
124	30.3	-95.9	23.32	22.95	22.73	0.41	0.75	2.50
125	80.9	-95.4		24.79				1.10
126	-46.8	-94.6		24.10				1.70
127	8.7	-93.1	22.92	21.38	20.14	1.48	2.79	3.90
128	95.7	-92.4		24.84				1.00
129	26.8	-92.2		24.15				1.70
130	-65.2	-92.2	24.28					
131	-31.5	-91.1	24.59	23.72		0.71		2.00
132	76.1	-90.4		24.81				1.10
133	177.9	-89.4	23.73	22.12	21.54	1.50		3.30
134	-84.4	-88.2		24.85				1.10
135	193.4	-87.9	21.99	21.51		0.47		4.20
136	86.6	-87.5	24.27		23.53		0.72	
137	-26.2	-87.0	22.86	21.59	21.29	1.18	1.52	4.00
138	83.1	-86.0		23.83				2.00
139	39.1	-85.8	22.47	22.65	22.19	0.15	0.43	2.80
140	139.9	-85.7	24.01	23.62	23.57	0.35	0.45	2.00
141	-96.1	-83.7	24.11	23.49		0.61		2.10
142	14.5	-83.0	24.66	23.22	23.11	0.98	1.40	2.60
143	-37.5	-80.9	22.71	21.84	21.53	0.81	1.16	3.30
144	65.4	-78.0	19.55	18.85	18.51	0.73	1.11	8.30
145	-70.9	-77.8	22.96	21.52	20.50	1.39	2.44	3.60
146	-9.1	-75.8	22.72	21.13	20.13	1.46	2.53	4.00
147	136.2	-75.6	24.12		23.99		0.11	
148	110.5	-71.4	24.24	23.34	22.90	0.68	0.92	2.40
149	49.7	-71.3	22.78	21.51	20.82	1.17	1.84	3.90
150	178.0	-71.0	21.75	20.55	29.61	1.12		4.90
151	-59.2	-69.9		24.46				1.50
152	167.5	-69.3	22.34	20.79	19.38	1.46	2.84	4.00
153	-6.7	-68.4		25.15				0.90
154	183.8	-68.2	24.15					
155	-33.2	-67.5		24.92				1.00
156	71.4	-66.9			23.70			
157	-95.7	-64.3		24.62				1.20
158	143.5	-63.3	20.81	19.86	19.27	0.99	1.58	4.90
159	25.4	-63.0	20.64	19.76	19.63	0.69	1.04	8.70
160	-87.5	-62.6		25.02				1.00

Table 3. continued

No.	X_{pix}	Y_{pix}	g	r	i	g-r	g-i	R_{iso}
161	-70.2	-61.9		24.50	24.19			1.30
162	-82.1	-61.5	24.27	23.76		0.44		1.90
163	85.7	-60.9	25.01					
164	-64.4	-60.1		23.87				2.10
165	-7.2	-58.1		25.15				0.90
166	66.7	-57.4		22.68	23.03			2.90
167	40.6	-57.2	20.02	18.95	18.39	1.08	1.82	9.90
168	101.7	-56.8	22.04	21.49	21.17	0.56	0.96	3.90
169	150.7	-55.7	21.10	20.20	19.42	0.94	1.76	5.30
170	-57.2	-54.9	20.63	20.03	19.71	0.64	1.00	5.30
171	74.2	-54.6	23.26	22.14	21.93	0.85	1.17	3.90
172	93.4	-53.5	24.18	23.00	22.67	0.96	1.36	2.50
173	-0.2	-52.8	23.11	22.30	22.05	0.61	0.91	3.60
174	29.2	-52.0	20.66	19.46	19.53	0.76	1.04	12.00
175	-57.2	-50.2	22.84	21.64	20.49	1.27	2.28	3.40
176	153.8	-50.2			24.41			
177	163.6	-50.0	23.16	22.30	22.04	0.79	1.02	3.30
178	-101.8	-49.7		24.32				1.60
179	-60.1	-45.3	20.48	19.62	19.50	0.81	1.24	7.40
180	-93.1	-43.2	24.70	24.87		-0.23		1.10
181	29.4	-40.6	18.39	17.52	17.43	0.77	1.09	
182	177.3	-39.3	23.52		23.91			
183	-29.7	-38.6	23.10	22.86	22.68	0.11	0.52	2.90
184	-62.8	-38.5			22.82			
185	-40.6	-37.1	23.04	22.33	21.91	0.66	1.10	3.20
186	164.6	-36.0	23.88	23.42	23.21	0.41	0.71	2.40
187	97.3	-34.9	22.56	21.89	21.49	0.59	1.04	3.90
188	149.6	-34.8	23.33	22.97	22.85	0.02	0.61	3.00
189	191.7	-34.4	25.04	24.42		0.39		1.40
190	-26.9	-33.0	24.67					
191	104.8	-32.9	22.22	21.74	21.24	0.58	1.05	3.70
192	-4.8	-32.1	22.98	22.38	22.00	0.50	0.96	3.30
193	-36.5	-29.0	23.07	22.21	22.02	0.91	1.14	2.80
194	144.2	-27.0	20.04	19.35	18.96	0.72	1.14	6.20
195	109.2	-26.7	24.95	23.13	22.11	1.39	2.45	2.30
196	131.4	-25.2			23.28			
197	170.0	-24.4		23.73	22.86			2.30
198	176.6	-24.4	24.55	23.73	23.78	0.64		1.90
199	4.6	-24.0	19.38	18.68	18.26	0.74	1.14	6.90
200	-83.9	-23.7	24.73	23.19	22.16	1.24	2.29	2.20

No.	X_{pix}	Y_{pix}	g	r	i	g-r	g-i	R_{iso}
201	-101.8	-22.8		19.46				5.80
202	-60.3	-22.6		24.40				1.50
203	127.6	-21.8	21.27	20.56	20.24	0.70	1.06	4.70
204	-11.5	-21.1		21.14	21.03			4.40
205	-25.0	-20.7	24.60	23.17	22.07	1.14	2.22	2.50
206	-6.9	-19.8	23.26	21.46	21.59	1.30	1.62	5.00
207	180.3	-18.3		24.69				1.20
208	-33.3	-17.5	21.47	21.18	20.78	0.33	0.69	3.90
209	75.1	-16.8	24.87					
210	201.4	-11.2		20.72				4.90
211	-53.0	-11.0	23.76	23.78	23.27	-0.09	0.54	2.00
212	-31.1	-9.3	24.47	25.05		-0.58		0.90
213	64.2	-7.5	21.14	20.85		-0.30		7.00
214	146.1	-7.3	24.22	23.18	22.86	0.70	1.04	2.60
215	74.0	-7.3	24.65					
216	-19.9	-6.3	23.29	22.85	22.53	0.47	0.79	2.60
217	9.9	-6.1	25.11					
218	185.1	-5.8	23.62	23.48		0.12		2.20
219	101.6	-5.3	22.81	21.81	21.70	0.89	1.08	3.60
220	-79.2	-5.3	20.39	19.78	19.47	0.65	0.95	6.80
221	116.5	-4.4			22.57			
222	201.5	-3.9		19.48				7.30
223	0.0	0.0	18.28	17.52	17.22	0.75	1.16	13.40
224	-13.3	0.1		21.37	21.25			4.20
225	-36.3	1.0		24.83				1.00
226	-53.2	2.8	24.56	25.20		-0.76		0.90
227	-89.8	3.9		24.92				1.00
228	89.4	4.3	24.19	23.74	22.66	0.64	1.58	1.80
229	-24.4	5.9	24.75	24.02		0.47		1.70
230	21.9	7.1	24.55	23.91		0.58		1.80
231	59.0	7.1	23.28	22.59	22.46	0.59	0.92	3.00
232	-60.3	7.6	24.23	23.09	22.72	1.04	1.44	2.30
233	-101.7	7.8		23.15				2.70
234	-1.2	7.8	21.22		20.13		1.07	
235	-10.7	8.6			21.98			
236	155.4	8.7	23.45	23.06	22.35	0.54	0.97	2.60
237	187.2	9.0		23.93				1.80
238	93.0	9.4	24.05		23.15		0.83	
239	41.3	11.5	20.64	19.72	19.54	0.75	1.07	7.70
240	62.5	12.2	23.18	22.94	22.58	0.35	0.78	2.70

Table 3. continued

No.	X_{pix}	Y_{pix}	g	r	i	g-r	g-i	R_{iso}
241	68.1	12.3	21.01	20.37	20.15	0.68	1.01	5.40
242	131.7	12.6	20.85	20.19	19.86	0.69	1.02	5.20
243	103.5	13.0		24.55				1.30
244	176.0	13.6	20.93	20.31	20.02	0.66	1.06	5.00
245	89.7	14.2	22.87	22.18	21.09	0.69	1.68	3.20
246	-82.9	15.9	17.95	16.93	15.97	0.98	1.87	9.70
247	-44.5	16.4	24.36	23.56		0.60		2.20
248	-34.9	17.5	24.52		23.08		1.17	
249	116.8	17.8		22.88	21.99			3.10
250	-29.4	19.1	22.99	21.48	20.38	1.32	2.45	3.90
251	8.9	19.5		24.88				1.10
252	121.9	20.4	23.50	23.22	22.86	0.30	0.74	2.30
253	-11.4	21.6	23.19	22.53	22.60	0.51	0.59	3.20
254	116.3	21.8	23.53					
255	158.5	22.6	23.87	23.80	23.70	-0.03		2.10
256	-98.4	22.6	19.47	18.85		0.75		7.30
257	96.0	23.4	23.49	22.69	22.54	0.59	0.95	2.90
258	-2.8	24.3	22.01	21.79	21.59	0.18	0.50	4.00
259	-34.2	26.6	22.02	21.33	20.98	0.68	1.02	3.90
260	24.6	27.1	23.82	23.16	22.94	0.34	0.79	2.80
261	41.9	27.7		25.13				0.90
262	72.3	28.0	23.36	22.46	21.88	0.77	1.17	3.00
263	-25.7	28.2	24.03	23.43	23.24	0.41	0.67	2.30
264	-73.9	28.4	20.15	20.06	19.90	0.14	0.29	4.80
265	-51.6	30.8		23.08	21.76			2.70
266	32.3	31.0	23.40	22.51	22.31	0.70	0.99	3.40
267	62.0	31.8	24.97	23.75	23.93	0.81	0.56	2.00
268	190.5	33.5	24.64					
269	166.0	34.8	20.29	19.31	18.80	1.02	1.54	6.70
270	19.9	34.8	24.48	23.69	23.22	0.52	0.94	2.00
271	195.2	35.1	23.49	22.50		0.94		2.80
272	109.8	36.4	24.89	23.27	22.62	1.13	1.87	2.50
273	33.3	36.6		24.85				1.10
274	-68.5	36.8	25.10					
275	-78.9	36.9	24.10	23.60		0.38		2.10
276	54.1	37.3	24.86	24.54		0.34		1.30
277	83.0	39.8		24.08				1.20
278	-10.0	41.3		22.75	22.68			3.20
279	37.1	41.3	25.28	24.15		0.59		1.60
280	181.6	41.6	22.71					
281	-65.1	42.3	22.68	21.63	21.23	1.01	1.45	3.60
282	-12.0	42.7	24.50		22.68		1.28	
283	145.5	43.6	18.68	17.99	17.57	0.75	1.18	11.10
284	-52.8	46.5	21.71	21.49	21.47	0.16	0.27	4.60
285	91.0	48.7	19.45	18.72	18.27	0.77	1.21	7.20
286	61.4	49.6	18.66	17.61	16.86	1.08	1.80	8.00
287	80.7	51.1	20.34	19.67	19.41	0.71	1.05	6.50
288	132.3	51.2	22.35	21.65	21.19	0.65	1.04	4.10
289	-10.9	51.5	17.99	17.84	17.63	0.17	0.41	8.00
290	118.6	52.5	23.33	22.99	22.83	0.18	0.61	2.70
291	-99.7	53.8		22.41				3.40
292	-55.0	57.6	24.34					
293	157.5	57.6	22.98	21.47	19.84	1.43	3.02	3.30
294	37.6	58.7	24.94	24.77	23.85	0.22	0.99	1.10
295	200.5	59.4		23.39				2.00
296	177.1	59.8	24.11					
297	15.8	60.1	24.04					
298	-67.9	61.0	22.80	22.24	21.97	0.52	0.82	3.30
299	-0.7	65.7	18.63	18.02	17.64	0.67	1.05	8.80
300	159.0	65.7	21.90	21.39	20.89	0.53	1.03	3.60
301	174.3	65.8	20.10	19.88	19.50	0.36	0.71	5.70
302	130.7	65.9	24.09	22.54	22.10	1.52	2.04	2.70
303	69.1	66.4	24.11	23.16	22.14	0.66	1.85	2.70
304	-13.6	67.2	22.00	20.30	19.85	1.58	2.15	6.00
305	-44.5	69.5	21.34	20.60	20.21	0.81	1.21	4.60
306	26.6	70.8	23.25	22.56	22.14	0.58	1.05	3.00
307	146.3	72.8	20.84	19.79	19.05	1.09	1.85	5.00
308	-94.2	73.1	25.10					
309	88.1	73.7	24.40					
310	60.3	73.8	23.96					
311	-86.2	74.6		24.94				1.10
312	-104.0	74.9		23.97				1.70
313	47.0	75.1	24.77	23.88	23.68	0.65	1.05	1.90
314	105.6	75.8	23.92	22.71	22.15	1.03	1.61	2.80
315	-30.9	75.8		23.79	22.72			1.90
316	186.2	76.8		24.21				1.70
317	74.5	77.0	20.73	20.09	19.71	0.70	1.08	4.90
318	-8.3	77.5		22.45	22.25			3.20
319	90.0	77.5			22.66			
320	-95.4	77.5		23.64				2.00

Table 3. continued

No.	X_{pix}	Y_{pix}	g	r	i	g-r	g-i	R_{iso}
321	55.1	77.5	22.95	22.68	22.47	0.18	0.57	3.30
322	94.5	78.0	23.30	22.81	22.31	0.37	0.87	3.10
323	178.6	78.5		23.97				1.80
324	-76.8	80.1	23.20	21.48	20.49	1.48	2.58	4.30
325	116.1	80.3	21.64	20.15	19.60	1.42	2.02	5.70
326	73.6	84.1	21.82	20.84	20.06	1.02	1.77	3.90
327	-9.3	86.2	21.62	21.29	20.76	0.39	0.89	4.50
328	-64.5	87.3	24.57	22.85	23.02	1.29	1.29	2.80
329	-45.2	87.4		25.15				0.90
330	-35.4	88.9	24.40	24.95		-0.24		1.00
331	17.9	93.1	21.86	22.02		0.01		3.80
332	-96.3	93.2	21.26	20.25		1.00		5.80
333	30.5	95.2	20.09	19.44	19.07	0.69	1.08	6.20
334	23.5	95.8		22.65	21.67			2.90
335	68.6	96.2	23.67	23.66		0.12		2.00
336	-42.4	98.0	24.75	23.26	22.08	1.16	2.48	2.40
337	1.9	98.2	18.28	17.75	17.41	0.65	1.07	12.30
338	80.1	99.8	20.00	19.31	18.94	0.68	1.07	7.50
339	93.3	101.0	23.82	23.42	22.89	0.50	0.91	2.00
340	-68.4	103.2		25.07				0.90
341	114.9	103.8			22.37			
342	36.3	105.4	24.67					
343	67.2	106.3	21.68	21.04	20.85	0.63	0.95	5.10
344	188.1	106.4	21.95	21.97		0.10		3.50
345	136.7	107.4	23.79	23.04	22.60	0.64	1.18	2.70
346	152.6	107.9	19.30	19.04	18.73	0.32	0.66	7.60
347	57.1	109.3	24.28	24.30	23.19	0.07	1.11	1.50
348	165.9	109.8		23.99				1.80
349	-86.2	110.8	24.03	23.15	22.83	0.95	1.37	2.50
350	12.7	111.3	20.73	20.12	19.83	0.64	1.01	5.70
351	1.4	111.9		24.61				1.40
352	199.8	112.3		24.46				1.40
353	-51.8	120.4	19.19	18.43	18.00	0.81	1.26	8.90
354	-73.2	123.3	24.48	23.70		0.56		2.20
355	176.5	124.3		24.19				1.70
356	29.9	125.2		24.13				1.50
357	162.7	125.6	22.24	21.38	20.85	0.86	1.37	4.30
358	-23.8	126.2	21.29	21.08	20.89	0.33	0.59	4.60
359	141.7	126.9	24.60	24.32		0.18		1.60
360	48.1	127.0		24.79				1.10

No.	X_{pix}	Y_{pix}	g	r	i	g-r	g-i	R_{iso}
361	-97.2	128.1	25.16					
362	76.0	129.9	21.43	20.86	20.55	0.55	0.93	4.70
363	-84.3	132.4	23.02	22.49	22.80	0.45	0.37	3.30
364	-14.5	134.0	25.27					
365	-58.2	135.4	19.21	18.57	18.17	0.68	1.12	8.00
366	44.3	135.8	23.87	22.22	21.73	1.26	1.85	3.60
367	17.6	138.3	21.16	19.94	18.87	1.21	2.27	4.70
368	141.7	140.2	22.60	21.69	21.56	0.72	1.00	3.90
369	100.5	142.1	22.44	20.92	19.54	1.44	2.80	3.90
370	-77.4	142.8	24.30	24.01		0.27		1.80
371	46.9	143.2	24.86		23.76		0.97	
372	-44.3	143.5		23.07	21.48			2.20
373	91.5	144.2	19.88	19.21	18.84	0.71	1.12	6.40
374	43.0	145.4		24.84				1.00
375	135.9	145.9		24.03				1.70
376	140.4	146.8	23.46	23.14	22.69	0.33	0.88	2.80
377	12.1	147.6		23.26	23.08			2.30
378	106.0	148.3	24.74					
379	-99.3	150.1		24.87				1.10
380	-33.9	150.3	17.88	17.82	17.58	0.09	0.35	7.80
381	142.3	150.4	24.79					
382	79.3	151.9	23.63	25.14	23.13		0.51	0.90
383	29.3	153.7		24.46				1.50
384	157.8	154.4	21.88	20.61	19.36	1.28	2.52	4.30
385	104.8	154.8	23.96	23.07	21.39	0.89	2.18	2.70
386	-91.2	156.6		25.10				0.90
387	167.4	156.7		24.65				1.20
388	-68.6	158.9	22.67	22.63	23.10	0.02	-0.21	3.50
389	7.8	160.7	24.64	24.34		0.21		1.60
390	-29.4	161.8	24.54	23.98		0.24		1.90
391	185.0	166.8	19.17	18.88		0.45		9.00
392	26.3	167.9	23.37	22.48	22.20	0.58	1.17	3.70
393	-97.6	168.1	22.08	21.21		0.92		4.20
394	-61.2	168.7	24.74	24.86		-0.21		1.20
395	31.9	171.2	21.26	19.91	19.42	1.34	1.89	6.90
396	-69.8	171.8	22.78	21.00	20.49	1.51	2.12	4.90
397	84.1	172.2	23.69	22.78	22.62	0.72	1.08	3.00
398	52.5	172.2	23.84	23.74	23.27	-0.11	0.56	2.30
399	184.6	172.8	21.26	20.22		1.13		5.30
400	118.5	173.2		24.03				1.80

Table 3. continued

No.	X_{pix}	Y_{pix}	g	r	i	g-r	g-i	R_{iso}
401	-73.3	173.5	22.99					
402	-17.0	176.8	19.40	19.22	18.96	0.22	0.53	7.60
403	114.8	179.8		24.84	23.94			1.10
404	-92.1	183.1	24.26	24.61		-0.17		1.40
405	-8.4	183.5	22.60	21.98	21.53	0.62	1.08	3.70
406	60.4	183.7	24.57	25.20		-0.48		0.90
407	203.7	184.0		21.11				4.40
408	-103.0	184.4		24.01				1.70
409	15.7	184.5	21.94	21.69	21.66	0.21	0.34	3.70
410	-30.2	185.1		24.48				1.50
411	175.7	185.9	24.05	23.46	22.70	0.42	1.12	2.20
412	133.3	186.6	20.07	19.46	19.18	0.65	1.00	6.90
413	52.1	188.9	24.60	24.23	22.49	0.26	1.78	1.50
414	188.7	189.1	24.81					
415	156.3	190.1	23.50	23.06	22.70	0.46	0.89	2.50
416	94.3	191.6	23.14	21.77	20.80	1.13	2.17	4.20
417	-97.0	192.1		23.54				2.10
418	75.2	192.1	24.38	23.95		0.13		2.00
419	-57.3	192.4	25.17					
420	-8.5	192.5	23.15	22.61	22.57	0.54	0.83	2.80
421	-103.3	194.4		23.65				2.20
422	198.3	199.8		21.30				3.70
423	36.8	201.1	24.69	23.71		0.56		2.20
424	183.3	201.8		24.27				1.60
425	-68.2	203.4	24.06	23.46		0.51		2.40
426	40.5	203.6	23.62	23.54		0.20		2.00
427	98.8	203.8		24.00				1.90
428	115.6	205.5	25.07	24.50		0.42		1.40
429	178.2	205.8	23.18	22.87		0.20		3.10
430	4.4	205.9	21.76	21.56		0.15		4.40
431	171.9	207.1	22.93	22.11		0.56		3.90
432	-50.7	207.5	24.48					
433	83.3	208.8	23.40	22.94		0.14		3.00
434	-42.3	209.2	25.08					
435	-90.0	209.5		24.92				1.00
436	139.8	211.1		25.11				0.90
437	-42.7	211.4		23.93				2.00
438	152.9	212.8	24.10	24.11		0.06		1.70
439	200.6	214.2		20.73				5.10
440	37.1	215.2	24.47	23.60		0.82		1.90
441	-48.5	216.5		24.29				1.60
442	135.7	218.8	24.53	23.90		0.28		2.20
443	-91.2	219.1		23.36				2.60
444	-7.6	219.9		23.90				1.90
445	-82.8	219.9		23.55				2.00
446	188.5	220.9		24.98				1.00
447	161.5	223.4	20.53	19.92		0.64		6.10
448	-66.3	224.3	21.58	20.10		1.47		4.80
449	74.6	225.8		22.49				3.00
450	41.3	226.2		24.02				2.00
451	159.8	228.8	22.24					
452	164.0	228.8	30.08					
453	-63.3	228.8	22.42					
454	-70.8	228.8	23.85					
455	41.5	-31.8	15.60	14.73	14.30			

Table 4. Catalog of the cluster A3305

No.	X_{pix}	Y_{pix}	g	r	i	g-r	g-i	R_{iso}
1	139.4	-309.0	22.24		22.71		-0.05	
2	-99.1	-308.2	22.55					
3	133.4	-308.1	23.10					
4	38.8	-306.2	24.42					
5	126.4	-300.2	23.32		21.79		1.34	
6	60.8	-299.6	21.10	20.37	20.19	0.77	0.99	4.80
7	144.7	-298.0	21.01	20.81	20.99	0.21	0.18	4.40
8	86.3	-294.6			21.96			
9	129.0	-291.9	22.22		21.58		0.83	
10	99.8	-286.9	20.32	19.45	18.96	0.91	1.23	6.40
11	-36.6	-286.5	22.79	21.75	21.70	0.97	1.16	3.60
12	-11.4	-284.9	18.45	18.05	17.83	0.46	0.68	9.50
13	-71.8	-281.2	23.85	22.83	22.38	0.97	1.43	2.50
14	-58.9	-280.4		22.25	21.81			3.00
15	76.6	-278.3	22.40	22.41		0.08		3.00
16	-105.6	-277.6	24.69					
17	-26.4	-277.1	21.09	19.85	19.12	1.21	1.98	5.10
18	-127.7	-276.5		21.07				3.80
19	39.3	-275.5	23.78					
20	-18.6	-273.7	22.65					
21	-61.4	-272.6	22.44	21.20	19.95	1.31	2.47	3.80
22	8.3	-271.7	23.07					
23	-69.2	-269.6	23.24		21.89		1.36	
24	105.3	-268.9	24.26					
25	-71.9	-268.5		23.01				2.30
26	95.0	-266.6	24.65					
27	17.3	-262.9	20.13	19.14	18.59	1.01	1.51	5.50
28	50.3	-260.1	25.03					
29	-2.2	-257.1	19.27	18.22	17.70	1.06	1.59	7.10
30	-68.5	-256.2	24.53					
31	142.4	-252.3	23.01	22.68		0.32		2.60
32	17.0	-251.2	24.62					
33	41.3	-246.8	22.80		22.19		0.96	
34	45.3	-246.6	22.42	21.07	20.97	1.14	1.45	4.90
35	-24.5	-245.2	23.27	22.80	22.69	0.76	0.98	2.60
36	-6.3	-243.7	24.41					
37	-57.7	-241.7	23.64	21.97	21.35	1.46	2.09	3.20
38	49.3	-241.7			22.55			
39	-65.7	-240.9	25.14					
40	64.5	-236.0	24.01					

No.	X_{pix}	Y_{pix}	g	r	i	g-r	g-i	R_{iso}
41	16.2	-235.1	25.12					
42	-90.5	-234.1	21.53	20.83	20.46	0.78	1.10	4.30
43	-86.6	-226.8	24.39					
44	-27.8	-225.2	23.43	22.07	21.78	1.11	1.55	3.60
45	11.7	-225.0	18.10	17.67	17.56	0.46	0.56	8.20
46	-39.1	-220.9	18.71	18.14	17.99	0.60	0.75	9.10
47	39.3	-219.4	24.71					
48	-101.5	-219.1	22.42	21.70	21.75	0.70	0.69	3.70
49	-53.3	-217.3	21.53	21.20	21.33	0.37	0.37	4.20
50	-36.7	-214.9	20.88					
51	31.9	-212.9			22.23			
52	-109.7	-212.6	23.92		22.40		1.46	
53	-78.7	-212.4	22.60	22.91		0.10		2.10
54	29.6	-210.5	23.13	22.02	21.34	1.00	1.53	3.20
55	109.6	-204.2	18.01	17.66	17.52	0.37	0.51	8.00
56	-33.1	-202.0	24.17					
57	136.3	-201.3	24.08					
58	32.9	-200.6	24.52					
59	67.0	-200.5	20.22	19.81	19.80	0.60	0.73	5.80
60	-118.4	-198.5	24.50					
61	124.5	-193.8	23.76	22.50	21.98	1.22	1.69	2.60
62	-124.7	-193.0	23.19	22.32	21.72	0.96	1.46	2.90
63	-26.5	-191.4	21.25	20.64	20.35	0.69	1.07	4.70
64	-77.8	-190.3	23.38					
65	-18.5	-188.5	24.92		21.85		2.44	
66	55.1	-186.8			22.16			
67	11.9	-184.7	24.26					
68	-107.6	-183.4	23.83					
69	-3.3	-180.8			22.42			
70	-79.6	-180.3	24.37					
71	127.0	-180.2	23.90		22.03		1.57	
72	138.7	-178.5	20.08	19.33	19.10	0.73	1.03	6.90
73	11.0	-174.9	25.05					
74	-54.0	-172.0	23.74					
75	-13.5	-171.6	21.11	20.65	21.11	0.48	0.48	6.40
76	-99.2	-170.1	24.88					
77	-31.5	-165.3	25.22					
78	-14.7	-156.6	22.77					
79	-42.0	-154.9	23.60					
80	136.2	-143.2	19.68	18.69	18.24	1.00	1.43	6.70

Table 4. continued

No.	X_{pix}	Y_{pix}	g	r	i	g-r	g-i	R_{iso}
81	59.6	-142.1	19.01	18.04	17.54	1.00	1.46	7.40
82	-59.7	-142.0	22.84					
83	-100.1	-139.9	24.98					
84	119.4	-139.1	22.48	21.98	22.06	0.52	0.61	3.50
85	147.7	-138.0	18.79	18.03	17.78	0.74	1.01	11.90
86	7.5	-135.1	21.30	20.94	20.82	0.31	0.52	4.50
87	97.8	-133.5	23.24	22.51	22.23	0.76	1.21	2.90
88	104.1	-128.5	23.63					
89	68.4	-125.6	24.97					
90	112.2	-123.4	24.97					
91	-42.3	-122.3	25.01					
92	126.5	-121.7	21.48	20.82	20.40	0.61	0.98	4.90
93	-111.3	-117.4	22.03	20.75	20.01	1.24	2.00	4.30
94	-93.1	-115.4		23.48				1.90
95	-95.3	-115.4	24.93					
96	48.4	-111.6	19.76	19.01	18.78	0.73	0.98	7.50
97	-74.3	-105.9	19.33	19.04	18.87	0.34	0.48	5.70
98	96.4	-101.6	24.73					
99	52.3	-98.2	25.05					
100	107.4	-97.3	24.36					
101	-11.4	-95.8	22.21	21.65	21.87	0.63	0.52	3.70
102	127.4	-94.5	24.04					
103	94.7	-92.7	22.71	22.24	22.38	0.65	0.55	2.80
104	-1.6	-91.7			23.05			
105	-4.0	-90.6	24.08	22.14		1.47		3.60
106	14.8	-90.6	22.62	22.04	22.16	0.64	0.62	3.20
107	68.5	-90.1	18.72	17.99	17.79	0.80	1.14	8.90
108	176.7	-88.7		21.75				3.50
109	-111.9	-87.8	19.97	19.37	18.94	0.72	1.04	6.80
110	-64.2	-86.5	20.33	19.65	19.44	0.71	0.98	6.20
111	71.0	-86.3	20.30		19.23		1.13	
112	146.5	-86.0	19.68	19.00	18.65	0.72	1.00	7.90
113	134.8	-85.0	23.47	22.90		0.55		2.60
114	-123.7	-84.6	18.73	18.07		0.54		15.00
115	-46.4	-84.4	18.75	18.32	18.06	0.50	0.79	8.40
116	116.4	-83.0	24.24					
117	-72.9	-82.4	22.35	21.95	22.78	0.29	0.07	4.10
118	-19.5	-79.9	24.63					
119	-70.6	-71.6	24.06					
120	-54.2	-68.9	20.86	20.13	19.86	0.73	1.00	5.10

No.	X_{pix}	Y_{pix}	g	r	i	g-r	g-i	R_{iso}
121	101.8	-67.5	23.91	21.94	21.17	1.65	2.49	3.50
122	64.4	-65.7	24.15					
123	73.0	-62.1	24.64					
124	-28.0	-61.7	24.17					
125	12.5	-60.9	23.18	22.40	22.58	0.83	0.90	2.90
126	-45.2	-60.8	22.07					
127	-62.7	-59.5			23.78			
128	-39.3	-59.4	22.75	22.61	23.08	0.22		2.60
129	-81.6	-58.9	23.63	23.06		0.81		2.50
130	-9.2	-58.6	23.20	21.64		1.43		3.80
131	-78.1	-56.7			23.29			
132	-56.8	-56.7	22.51	21.78	21.22	0.64	1.26	3.90
133	153.2	-56.6	23.83	22.26	21.02	1.39	2.71	3.00
134	-52.6	-56.5		21.97				3.70
135	-117.8	-56.2			22.08			
136	-12.2	-54.0			22.64			
137	174.7	-53.0		19.78				4.90
138	-123.6	-52.4	22.16	20.99	20.14	1.18	2.01	3.80
139	90.0	-46.1	23.66	22.97		0.77		2.40
140	53.3	-42.9	18.35	17.59	16.97	0.79	1.11	13.00
141	-118.1	-38.9			22.63			
142	74.6	-38.6	23.68	22.49	21.66	1.33	2.17	2.50
143	86.3	-37.8	23.81	22.60	21.21	0.91	1.75	2.90
144	-41.0	-35.4	21.08	20.43	19.87	0.72	1.19	4.90
145	76.3	-31.8	23.51	23.13		0.28		2.20
146	-104.0	-30.9	24.06					
147	-15.3	-29.6	23.18	22.91		0.46		2.60
148	40.9	-29.4	17.84	17.13	16.69	0.54	0.98	
149	34.2	-27.5	17.35	16.45	15.96	0.82	1.01	18.20
150	-55.9	-26.7	24.08	22.85		0.76		3.00
151	54.0	-24.9	20.02	19.27	18.91	0.75	1.06	6.60
152	128.9	-24.0	24.67					
153	149.2	-23.2			22.09			
154	-102.1	-22.2	24.15					
155	-14.4	-19.6			22.27			
156	72.4	-17.7	24.13					
157	45.3	-16.6		20.47				8.50
158	117.8	-15.6	24.34					
159	-82.1	-13.2	23.85					
160	87.9	-13.2	25.04					

Table 4. continued

No.	X_{pix}	Y_{pix}	g	r	i	g-r	g-i	R_{iso}
161	47.6	-12.2	22.17	21.76		0.58		3.90
162	32.0	-11.6	20.74	19.96	19.33	0.70	1.01	6.70
163	-110.9	-11.0	24.41	23.29	22.92	0.92	1.26	2.00
164	70.6	-9.5	19.40	18.77	18.43	0.70	1.03	8.60
165	144.6	-6.3	25.13					
166	-5.4	-6.3	22.19	20.87	20.47	1.32	1.69	4.30
167	-32.2	-4.8	21.86	21.04	21.12	0.73	0.80	4.50
168	-28.2	-4.5	21.25	20.32	20.26	0.75	0.96	6.30
169	-16.1	-3.6	23.25		22.26		0.75	
170	32.8	-2.6	21.41	20.80	20.55	0.72	0.93	4.60
171	9.8	-1.4	20.21	19.29	19.06	0.78	1.10	10.20
172	122.6	2.1	25.10					
173	43.1	2.3	21.99	21.35	20.72	0.69	1.15	3.80
174	4.0	2.4	19.89	19.11	19.09	0.85	1.00	6.50
175	76.5	2.6	24.90					
176	57.4	4.0	19.58	18.51	18.19	1.16	1.52	9.10
177	-47.2	5.4	20.26	19.57	19.35	0.72	0.98	6.00
178	8.9	7.2	18.26	17.49	17.16	0.84	1.16	11.80
179	80.0	8.0	22.88	22.37	22.15	0.51	0.86	2.90
180	-90.1	12.1	23.55					
181	136.5	13.3			22.74			
182	94.7	18.3	21.55	20.84	20.80	0.68	0.84	4.70
183	-107.3	19.6	21.28	20.54	20.18	0.86	1.23	5.10
184	86.8	19.8	24.63					
185	11.1	21.0	19.43	18.70	18.38	0.76	1.05	8.70
186	-65.1	25.6	19.79	19.11	18.83	0.71	0.98	6.80
187	-52.7	26.3	25.13					
188	-113.7	27.2	22.20	21.32	20.96	1.00	1.40	4.10
189	86.2	27.4			22.11			
190	-109.7	28.4			22.81			
191	-0.9	28.7		23.24	22.44			2.20
192	-12.1	29.0	23.93		23.22		0.92	
193	125.3	29.3	24.96					
194	34.0	32.0	18.10	17.36	17.06	0.78	1.03	11.90
195	-28.7	32.1	23.05		22.59		0.80	
196	67.4	32.6	22.69					
197	-79.1	33.1	21.08	20.00	19.71	1.08	1.41	5.70
198	109.0	33.4	22.78		22.14		0.89	
199	111.5	33.5		21.72				3.70
200	20.7	34.6	20.71	19.99	19.87	0.75	0.94	5.80

No.	X_{pix}	Y_{pix}	g	r	i	g-r	g-i	R_{iso}
201	-32.8	36.2		22.16	21.65			3.70
202	-34.7	36.4	23.42		21.65		1.53	
203	90.4	36.6	22.72	22.36	21.55	0.35	1.05	2.80
204	-119.9	38.8	23.37	22.66	22.55	0.67	0.94	2.80
205	165.9	38.9		23.27				1.70
206	-58.2	40.9	23.33	22.79		0.60		2.70
207	4.1	42.1	20.03	19.37	19.05	0.71	1.00	6.50
208	23.3	42.5	23.47					
209	-7.8	42.7	22.27	21.04	20.66	1.16	1.53	4.30
210	53.2	43.9	18.68	18.41	18.38	0.27	0.30	8.10
211	125.8	44.4	25.06					
212	149.5	46.5			22.56			
213	9.3	46.7		21.98	21.88			3.40
214	143.9	50.1	22.86	22.65	22.64	0.43	0.45	2.30
215	12.1	54.2			23.01			
216	170.7	57.3		19.94				5.60
217	53.9	57.7	24.75					
218	-130.3	58.7		21.47				4.30
219	9.9	65.8	23.36					
220	94.7	66.4			22.83			
221	-58.9	66.5	22.97	21.92	21.99	0.89	0.98	3.60
222	-7.0	68.3	18.87	18.08	17.79	0.78	1.06	11.20
223	121.4	69.3	22.05	21.33	21.14	0.67	0.88	4.00
224	60.3	69.3	24.99					
225	36.5	70.9	24.06					
226	-29.2	72.7	21.47	20.79	20.59	0.68	0.85	4.70
227	121.4	75.4	23.67					
228	12.4	79.2	19.99	18.89	18.50	1.08	1.49	7.90
229	142.6	80.3	18.91	18.31	18.12	0.61	0.81	7.50
230	33.8	82.2	23.00	22.24	21.69	0.67	1.13	3.30
231	-78.7	83.1	22.59	21.64	21.73	0.78	0.86	4.30
232	110.1	85.6	23.60	21.98	20.82	1.39	2.53	3.60
233	8.7	87.3	21.98	21.23	20.96	0.78	1.11	4.00
234	-38.5	90.0	23.37	21.38	20.89	1.76	2.21	4.20
235	-25.2	90.7	22.58	21.61	21.27	0.91	1.29	3.70
236	-66.0	92.3	22.10	21.78	21.47	0.29	0.58	3.60
237	-70.7	92.4			21.27			
238	41.7	93.1	24.73					
239	148.4	99.4	22.55	22.26	22.12	0.36	0.60	3.20
240	164.8	99.8	22.54	22.18	21.80	0.35	0.74	3.00

Table 4. continued

No.	X_{pix}	Y_{pix}	g	r	i	g-r	g-i	R_{iso}
241	-5.6	103.2	21.77	20.69	20.39	1.07	1.38	4.70
242	129.5	103.3	24.74					
243	-51.6	106.7	23.73					
244	-101.8	107.9	18.75	17.95	17.62	0.85	1.18	10.60
245	143.6	111.0	20.92	19.75	19.07	1.15	1.81	5.10
246	76.5	112.7	20.57	19.84	19.57	0.73	1.02	5.90
247	-51.7	119.8	21.79	20.83	20.49	1.00	1.32	4.60
248	-4.1	121.1	23.52					
249	174.5	121.4		21.86				3.20
250	124.0	123.8			23.12			
251	144.5	124.0	24.69					
252	-36.6	125.1	24.97					
253	84.1	125.8	24.63					
254	-26.3	126.0	20.82	20.06	19.87	0.73	0.95	5.80
255	48.7	127.2	19.83	19.05	18.74	0.77	1.07	6.80
256	31.1	129.5	20.43	19.79	19.45	0.67	0.92	5.90
257	14.5	130.7	23.30	22.21	21.80	1.00	1.52	3.30
258	168.3	131.2	25.11					
259	70.4	135.4	23.81					
260	122.3	142.3			23.31			
261	129.3	142.3	24.86					
262	-104.1	144.1	23.87	22.68	21.56	1.00	1.71	2.60
263	142.1	145.8	23.90					
264	-12.1	145.9	23.27	23.03		0.33		2.50
265	-116.9	150.2	22.88	22.14	22.08	0.75	0.92	3.30
266	-21.9	159.2	21.30	20.32	19.91	0.97	1.33	4.80
267	87.2	161.4	19.23	18.92	18.82	0.34	0.44	6.40
268	21.8	162.5	19.81	19.19	18.89	0.70	0.98	6.60
269	117.8	164.3	22.67	21.72	21.48	0.92	1.10	3.90
270	13.5	165.2	20.23	19.01	18.19	1.22	2.02	6.10
271	-91.8	166.0	20.78	20.00	19.70	0.84	1.12	4.90
272	-31.7	166.5	23.19	22.16	21.86	1.06	1.36	3.20
273	-1.7	168.8	20.22	20.05	20.06	0.18	0.18	5.00
274	-67.4	174.1	21.54	20.62	20.34	0.94	1.23	4.90
275	-120.5	179.5	23.86	22.98		0.22		3.10
276	177.0	179.8		18.79				5.60
277	102.5	181.8		21.64				4.00
278	77.5	181.8		23.02				2.70
279	15.9	182.0		23.69				1.70
280	23.1	184.4		22.85				1.70
281	180.3	185.4		20.85				4.40

Table 5. Catalog of the cluster A1942

No.	X_{pix}	Y_{pix}	g	r	i	g-r	g-i	R_{iso}
1	90.1	-330.0			23.09			
2	-136.7	-329.9	23.98	23.22		0.56		1.40
3	-63.7	-319.5		22.23	21.87			2.10
4	-4.1	-316.0	23.26	22.71	22.41	0.58	0.95	1.80
5	54.8	-313.6	22.48	22.06	22.08	0.37	0.55	2.50
6	-45.2	-312.6	23.45	23.57		-0.01		1.10
7	36.7	-307.8	22.58	22.92		-0.22		1.60
8	19.1	-305.2	22.21	21.33	20.95	0.81	1.23	2.90
9	-36.7	-297.7	23.33	22.26	22.36	0.86	0.99	2.10
10	123.1	-293.9	23.12	23.48		0.00		1.20
11	-101.8	-293.4	21.87	20.74	20.16	1.02	1.64	3.10
12	-131.8	-292.1	23.15	22.04	21.00	0.78	1.77	2.40
13	148.6	-282.5		23.54				1.10
14	-44.6	-281.1		23.69				0.90
15	-119.9	-277.2	22.37	21.05	20.10	1.00	1.89	3.40
16	4.4	-273.4			23.04			
17	-65.7	-271.5	23.88	22.48	22.21	0.88	1.31	1.90
18	-75.4	-267.8	23.25	21.27	21.13	2.31	2.46	3.00
19	48.4	-267.0	23.53		22.10		1.10	
20	66.6	-262.5	22.85	23.12		-0.13		1.50
21	99.8	-260.0	23.95					
22	64.4	-252.7	21.89	20.41	20.18	1.22	1.52	4.20
23	-49.7	-252.7			22.37			
24	87.7	-249.5		22.86	21.55			1.70
25	-98.2	-249.3	20.62	19.77	19.44	0.81	1.15	3.80
26	161.9	-238.2	23.39					
27	66.9	-237.2		22.99	21.84			1.70
28	-38.2	-230.8	23.20	22.10	21.17	0.89	1.75	2.10
29	59.4	-225.9	23.15	21.64	20.56	1.28	2.35	2.60
30	14.5	-222.8	24.02	22.75	22.53	0.92	1.20	1.70
31	-2.8	-222.7	19.38	18.78	18.63	0.59	0.77	6.20
32	24.8	-222.5	19.70	18.79	18.57	0.87	1.13	5.90
33	-104.0	-220.7	22.10	21.31	21.17	0.66	0.90	3.00
34	49.2	-212.4		23.89				0.90
35	29.3	-212.3		23.56				1.00
36	-49.4	-202.9	21.60	21.27	21.24	0.29	0.39	3.00
37	36.1	-202.6	24.10	22.52	22.55	1.24	1.38	1.80
38	141.8	-202.3	22.32	21.23	20.54	1.01	1.70	3.00
39	-17.7	-200.2	23.22	21.88	22.29	0.80	0.95	3.00
40	-59.9	-200.0	22.54	21.62	21.70	0.76	0.77	2.90
41	-119.0	-195.7	19.56	19.54	19.59	0.02	0.00	4.20
42	17.3	-193.6	20.50	19.71	19.46	0.78	1.05	4.50
43	102.2	-191.9	22.71					
44	157.0	-188.5	23.59					
45	12.4	-183.0		23.88	22.86			0.90
46	104.2	-182.9	22.65	21.60	21.44	0.84	1.16	2.90
47	-129.8	-182.8	22.76	21.53	20.56	1.06	1.96	2.70
48	-118.0	-182.1		23.80	22.87			0.90
49	-107.8	-180.3	23.53					
50	119.6	-179.0			23.19			
51	-86.0	-177.2		23.84	23.19			0.90
52	-125.4	-177.1	22.38	21.18	20.91	1.00	1.40	3.20
53	-26.5	-175.6		23.59				1.10
54	-77.3	-174.8		23.24	22.93			1.40
55	118.9	-166.7	20.44	19.51	19.30	0.84	1.10	5.50
56	162.4	-164.1		22.85	22.57			1.60
57	-48.1	-162.3	20.76	20.94	20.90	-0.13	0.05	3.70
58	66.6	-159.7	20.88	20.14	19.93	0.72	0.96	4.00
59	-109.0	-159.3	23.44	22.40	21.94	0.87	1.42	1.90
60	69.9	-154.8	21.56	20.61	20.38	0.86	1.18	3.80
61	108.5	-151.6	22.58	21.96	22.32	0.66	0.60	2.50
62	0.6	-148.1	20.51	19.61	19.36	0.85	1.13	5.00
63	-15.0	-148.0	23.08	22.06	21.70	0.89	1.37	2.30
64	-8.8	-143.8	22.44	21.43	21.19	0.86	1.19	2.90
65	17.0	-142.0		22.58	23.08			1.90
66	12.4	-139.7	21.87	21.08	21.14	0.68	0.82	3.50
67	-85.1	-137.8	16.26	15.94	15.83	0.26	0.36	18.70
68	-2.1	-133.5	24.09	22.99		0.76		1.60
69	139.8	-132.4	21.54	20.79	20.60	0.71	0.98	3.50
70	25.4	-132.2	20.62	20.24	20.08	0.39	0.59	3.80
71	34.6	-131.2	22.73	21.56	21.28	0.96	1.30	2.90
72	-74.5	-131.1		19.57				6.10
73	9.6	-130.0	19.61	19.08	18.88	0.50	0.72	5.90
74	108.3	-127.3	20.27	19.46	19.23	0.78	1.05	5.30
75	-118.9	-123.5	19.17	19.61	19.83	-0.43	-0.60	4.20
76	149.2	-123.1		23.17				1.50
77	5.8	-122.3			23.01			
78	91.4	-121.5	20.23	19.36	19.10	0.83	1.10	5.10
79	-67.2	-119.0	22.36		21.68		0.75	
80	-35.7	-111.2		23.59				1.10

Table 5. continued

No.	X_{pix}	Y_{pix}	g	r	i	g-r	g-i	R_{iso}
81	-111.5	-111.2		22.33	21.88			2.10
82	-57.2	-110.9	23.90					
83	115.4	-108.8		22.91	23.18			1.70
84	-119.6	-104.6		22.51	23.00			2.10
85	-48.2	-104.4		23.75				1.00
86	-108.9	-103.2	21.17	20.37	20.14	0.75	1.05	3.70
87	120.9	-102.4			22.85			
88	-82.5	-102.3	22.81	22.77		0.16		1.80
89	-25.3	-101.0		23.54				1.10
90	45.6	-101.0	18.81	18.56	18.48	0.26	0.35	4.90
91	125.6	-97.6	20.80	19.90	19.63	0.85	1.13	4.10
92	-46.6	-95.3	22.74	21.74	20.52	0.97	2.12	2.40
93	149.6	-93.7		22.83	21.96			1.80
94	-80.8	-91.8	23.23	22.06	22.09	0.88	1.02	2.50
95	162.0	-91.5	23.44					
96	88.0	-90.0		21.92				2.90
97	119.8	-89.7	23.69	23.63		0.33		1.00
98	12.8	-87.1	21.41	20.65	20.55	0.71	0.87	3.80
99	143.7	-86.6	19.16	19.21	19.18	-0.05	-0.01	4.30
100	-46.9	-86.6			23.00			
101	79.8	-84.8	18.77	17.75	17.48	0.88	1.22	11.60
102	3.6	-84.0	20.94	20.00	19.73	0.93	1.22	4.00
103	22.1	-83.2		22.80	22.42			1.70
104	-6.8	-82.9		22.20	21.13			2.60
105	-58.4	-82.3	20.50	20.40	20.48	0.11	0.11	3.70
106	160.9	-81.5		22.66				2.10
107	-53.8	-81.5			22.84			
108	112.1	-81.0	22.20	22.50	22.35	0.02	0.23	1.90
109	151.7	-77.8	21.30	20.70	20.49	0.59	0.78	3.60
110	153.4	-73.3	21.49	20.56	20.31	0.84	1.10	3.80
111	15.0	-67.8	23.90	22.31	22.19	0.87	1.15	2.30
112	-82.6	-67.1	20.85	20.05	19.86	0.76	0.97	3.90
113	84.8	-65.2	23.79					
114	-124.6	-60.6	20.97	20.19	19.90	0.77	1.10	4.00
115	-45.8	-60.6	21.22	19.97	18.83	1.17	2.28	3.80
116	83.1	-56.8	22.04	21.02	20.86	0.90	1.12	3.30
117	44.8	-56.6	20.27	19.52	19.30	0.73	0.99	5.20
118	-28.5	-55.2			22.80			
119	96.7	-54.8	21.76	21.64	21.80	0.07	0.38	3.10
120	23.1	-51.3	22.17	21.74	21.71	0.34	0.52	2.70
121	-7.9	-51.3	21.45	20.52	20.34	0.77	1.06	4.00
122	5.9	-50.8		23.50	23.10			1.20
123	67.0	-49.7	20.56	20.48	20.52	0.09	0.13	3.80
124	114.8	-49.3	21.26	20.57	20.44	0.67	0.93	3.90
125	13.9	-49.3		23.81				0.90
126	-94.7	-45.5	20.81	20.05	19.88	0.69	0.90	4.80
127	105.5	-43.6	22.36	21.24	20.87	1.10	1.48	2.80
128	39.3	-43.1		23.22	22.82			1.40
129	-34.2	-42.4		22.80	22.45			1.80
130	-2.1	-39.6	19.50	18.54	18.29	0.90	1.18	6.80
131	97.4	-37.4	20.84	19.93	19.63	0.84	1.16	4.20
132	-25.8	-34.1	19.92	19.09	18.82	0.80	1.10	5.40
133	33.4	-33.4	20.68	19.80	19.59	0.83	1.07	4.30
134	126.7	-33.0	19.90	19.06	18.77	0.82	1.12	5.60
135	49.3	-32.3	20.36	19.23	18.89	1.06	1.42	5.80
136	106.7	-30.0	24.00					
137	159.3	-27.7		23.54				1.10
138	-69.6	-26.5	21.45	20.46	20.28	0.90	1.10	3.70
139	-17.0	-26.3	22.10	21.22	20.88	0.67	1.09	3.20
140	85.4	-24.7	21.98	21.75	21.86	0.28	0.34	2.60
141	-8.2	-24.7	20.20	19.32	18.83	0.87	1.35	4.30
142	-44.7	-24.4	22.13	20.99	20.52	1.06	1.53	3.00
143	102.5	-24.2		23.79				0.90
144	24.8	-24.0	20.78	19.92	19.76	0.81	1.05	4.90
145	162.6	-23.0	23.33	22.20		1.20		2.20
146	-138.8	-22.3	20.68	19.76	19.42	0.88	1.23	4.40
147	27.3	-19.5	24.01					
148	63.9	-17.9		23.79				0.90
149	10.2	-16.3		23.72				1.00
150	-102.9	-15.7			23.07			
151	102.2	-15.6	21.93	21.20	21.10	0.68	0.86	3.30
152	-79.6	-15.5	22.28	21.92	21.97	0.39	0.50	2.50
153	-36.0	-13.9	20.94	19.74	19.40	1.16	1.51	5.10
154	51.7	-12.1	19.53	19.22	19.12	0.30	0.46	5.80
155	39.7	-12.0	21.47	20.60	20.37	0.79	1.07	3.80
156	61.7	-11.1		22.67	22.59			1.90
157	148.9	-10.3	20.66	19.90	19.60	0.73	1.06	4.30
158	24.5	-6.9		23.12	22.57			1.50
159	16.3	-5.7	23.88	22.23	22.20	1.30	1.46	2.10
160	2.8	-5.6	19.46	18.39	18.21	0.97	1.20	7.10

Table 5. continued

No.	X_{pix}	Y_{pix}	g	r	i	g-r	g-i	R_{iso}
161	-34.5	-5.3	21.04					
162	-102.2	-4.4	20.36	19.87	19.63	0.47	0.74	4.30
163	82.3	-3.7	22.80	21.61	21.91	0.69	0.86	3.20
164	-13.6	-2.7	21.61	20.50	20.28	0.98	1.25	3.80
165	11.9	-2.4	23.85					
166	-35.8	-2.2	20.79	19.92	19.16	0.81	1.17	4.70
167	-76.4	-1.6	18.84	18.26	18.08	0.58	0.81	7.60
168	-31.0	0.2	21.18	21.05	21.56	0.16	-0.20	3.30
169	32.9	1.0	23.54	21.97	21.77	1.34	1.58	2.30
170	-6.4	1.7	20.93	19.88	19.71	1.06	1.22	3.90
171	112.2	5.9		22.69	21.53			1.80
172	-42.7	6.2	23.19	22.15	22.44	0.87	0.87	2.20
173	26.0	7.5			22.75			
174	-127.9	8.8	23.90	22.87	21.73	0.96	1.95	1.70
175	27.4	10.0	23.92	23.01		0.36		1.60
176	-1.1	10.5	22.19	20.62	19.52	1.20	2.23	4.00
177	-88.4	10.9		22.72	22.63			1.90
178	88.9	12.8	21.80	21.37	21.32	0.34	0.60	3.10
179	76.8	13.9	22.89	22.10	21.22	0.58	1.42	2.30
180	72.3	14.1		23.73				1.00
181	-8.1	17.8		18.94				9.00
182	93.6	18.4	23.72	21.90		1.46		2.80
183	105.6	20.8	23.07	21.79	21.76	1.03	1.30	3.00
184	-8.0	21.5			18.11			
185	30.0	23.1	22.24	21.41	21.24	0.72	0.97	2.90
186	-55.6	23.2	22.39	22.65	22.58	-0.10	0.23	1.90
187	121.2	24.5	20.73	20.65	20.43	0.12	0.41	4.00
188	-8.0	24.8	20.62	19.43		0.91		6.70
189	-18.6	26.3	18.01	17.06	16.88	0.85	1.13	13.50
190	74.0	26.8	21.50	20.83	20.69	0.51	0.73	3.60
191	-80.6	30.7		23.89				0.90
192	104.1	31.4	19.32	18.49	18.18	0.82	1.14	7.20
193	2.6	31.6	22.73	21.61		0.98		2.80
194	-110.5	32.1	23.55	23.16	23.18	0.37	0.61	1.40
195	-104.4	35.1		23.67				1.00
196	-28.0	36.7	19.94	19.06	19.12	0.81	0.93	7.00
197	66.5	38.5	21.45	20.97	21.05	0.41	0.52	3.70
198	20.4	39.8	21.49	20.42	20.07	0.96	1.33	3.90
199	98.3	41.6	19.88	19.11	18.80	0.76	1.08	5.50
200	114.7	42.5	21.71	21.14	21.06	0.45	0.67	3.30

No.	X_{pix}	Y_{pix}	g	r	i	g-r	g-i	R_{iso}
201	-86.9	42.6	21.89	21.38	21.20	0.50	0.79	3.00
202	17.7	43.4			22.71			
203	-35.5	44.1	22.53	21.37	21.37	0.91	1.04	3.00
204	35.1	44.6		23.77				1.00
205	-53.5	45.8	19.33	19.30	19.30	0.03	0.05	4.40
206	126.7	48.1	23.71					
207	26.1	50.1	23.78	23.05	22.85	0.75	1.18	1.60
208	-28.4	50.9	21.10	20.17	20.03	0.86	1.06	4.20
209	67.9	51.4	17.97	17.52	17.39	0.44	0.57	6.20
210	-96.0	54.4	23.78					
211	54.5	55.1	23.63					
212	-96.6	58.3			22.06			
213	142.9	59.2	23.52					
214	32.0	61.1	22.55	21.45	21.36	0.81	1.07	3.20
215	-119.9	64.3	23.04	22.18	21.73	0.63	1.16	2.50
216	9.1	64.7	20.54	19.38	18.51	1.09	1.96	4.50
217	-14.4	65.0	22.66	22.51		0.21		1.90
218	-12.0	65.6			22.61			
219	-64.5	66.3	21.78	20.97	20.64	0.75	1.10	3.30
220	-35.1	68.4	23.72	22.93	23.00	0.43	0.68	1.60
221	-94.8	68.6	23.99	21.96	20.65	1.38	2.59	2.30
222	-15.7	69.7		23.29				1.40
223	-111.3	71.3	20.10	19.64	19.45	0.47	0.67	4.80
224	-87.6	72.0	23.73					
225	-82.2	72.7	23.85	23.00	23.12	0.76	0.89	1.60
226	-5.7	74.0		23.24				1.40
227	-0.5	74.0	19.96	20.05	19.98	-0.07	0.04	4.10
228	3.7	78.6		23.38				1.00
229	-21.2	79.7	22.88	21.85	21.62	0.79	1.07	2.70
230	11.7	80.3	23.36					
231	-57.7	81.5	20.55	19.65	19.39	0.85	1.12	4.50
232	152.6	85.0			22.31			
233	9.3	86.4	20.11	19.21	18.93	0.86	1.16	5.50
234	-100.4	90.0	20.04	20.45	20.58	-0.35	-0.32	3.70
235	116.6	90.5	20.31	19.29	18.49	1.00	1.78	4.10
236	-105.0	93.4	21.13	21.03	20.86	0.11	0.34	3.00
237	63.4	95.4	22.04	22.29	22.45	-0.03	0.12	2.30
238	1.3	96.2	21.55	21.46	21.46	0.10	0.19	2.70
239	109.4	101.9	19.29	18.51	18.23	0.77	1.09	7.10
240	147.7	103.7	22.37	22.06	22.31	0.31	0.30	2.40

Table 5. continued

No.	X_{pix}	Y_{pix}	g	r	i	g-r	g-i	R_{iso}
241	121.0	103.7	21.19	20.39	20.14	0.77	1.06	4.10
242	-89.0	103.8	20.79	20.07	19.83	0.70	0.99	4.30
243	-45.4	104.5		23.20	22.99			1.40
244	22.6	105.8	23.12					
245	-36.5	107.8	24.04	23.31		0.79		1.40
246	106.8	109.9	22.05	21.89	22.15	0.14	0.37	2.80
247	105.6	116.1		22.16	22.13			2.20
248	147.1	118.4	22.17	21.73	21.56	0.42	0.70	2.70
249	-83.0	118.9	22.23	22.81		-0.27		1.80
250	24.8	123.5	20.78	20.03	19.74	0.74	1.06	4.00
251	47.0	123.6	19.68	19.04	18.73	0.71	1.02	6.00
252	-134.0	126.3	23.19	21.95	21.03	0.85	1.73	2.50
253	-4.3	126.5		23.52	22.37			1.10
254	-96.6	126.7	21.57	21.30	21.32	0.33	0.49	3.50
255	-33.5	128.0	21.38	20.63	20.37	0.66	0.99	3.70
256	-62.5	128.1	23.70	22.64	22.27	0.81	1.39	1.80
257	15.6	128.4	20.48	20.11	19.87	0.37	0.64	3.80
258	-17.0	129.8		23.61				1.10
259	5.4	132.4	23.85	22.57	22.38	0.78	1.14	1.90
260	46.0	132.4		22.77				1.90
261	92.0	136.8		15.75				11.10
262	138.9	136.9	19.61	18.94	18.57	0.66	1.03	4.70
263	-60.7	140.0	21.91	22.05	21.48	0.14	0.73	2.40
264	72.3	140.0		22.33	22.79			2.40
265	8.6	142.2	23.51	22.49	21.73	0.92	1.68	2.00
266	-82.0	142.6	22.92	22.36	22.07	0.39	0.88	2.30
267	66.9	144.6	22.72					
268	25.7	147.2	22.29					
269	-83.7	148.8	22.56					
270	-55.9	149.0	19.65					

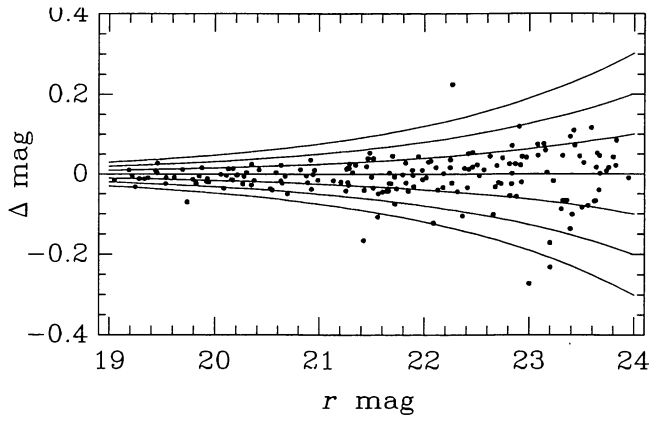

Fig. 1. Error distribution from repeated r-photometry for 174 objects detected in the 900 s frame of A3284 (see text for computational details). The $\Delta = k\sigma_{22}10^{0.2(r-22)}$ curves are for $k = \pm 1, \pm 2$, and ± 3 while $\sigma_{22} = 0.04$ mag is the Poissonian standard error at $r = 22$

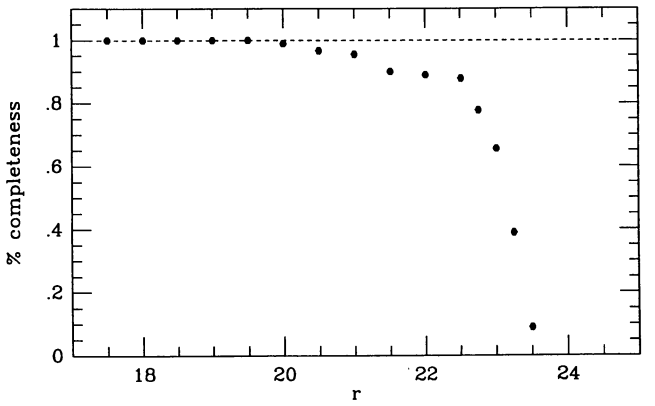

Fig. 3. Selection function in the photometry. Plotted are the results of a test on the r frame of A1942 with a magnitude limit $r_{\rm lim} = 23.5$. A bright unsaturated object in the frame (No. 90 in Table 5) has been singled out as a reference image (after removing local sky), and randomly re-added with an appropriate flux rescaling in order to simulate test objects of different magnitude. The efficiency in the object recognition has been tested then by running INVENTORY over 1,000 trials

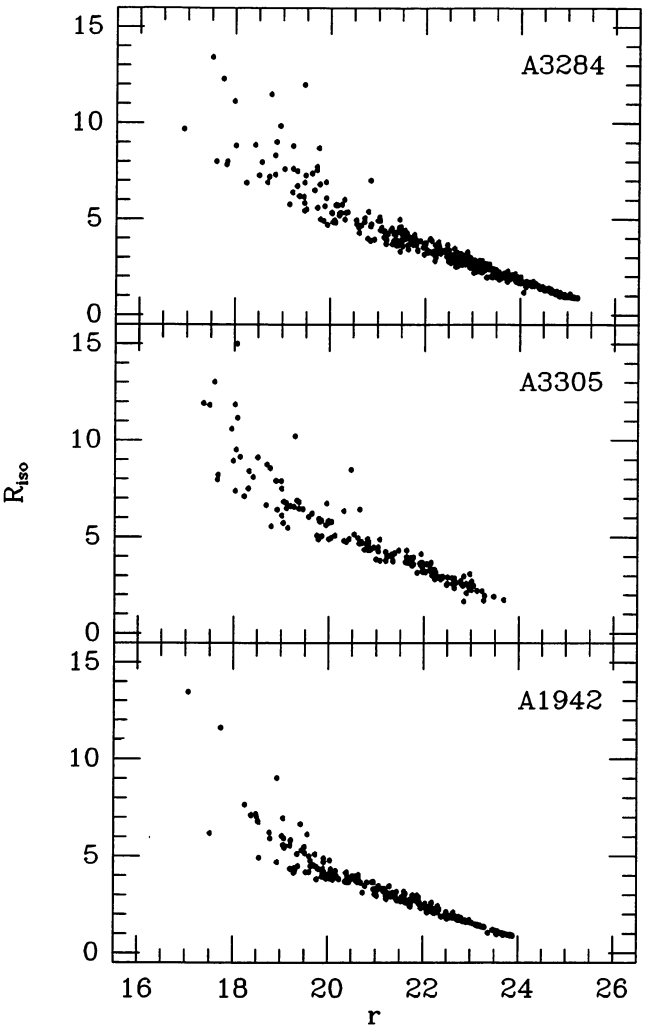

Fig. 2. Isophotal radius $R_{\rm iso}$ (in pixels) vs. r magnitude for the objects measured in the field of the three clusters. Galaxies more extended than the point spread function display a larger radius at fixed magnitude

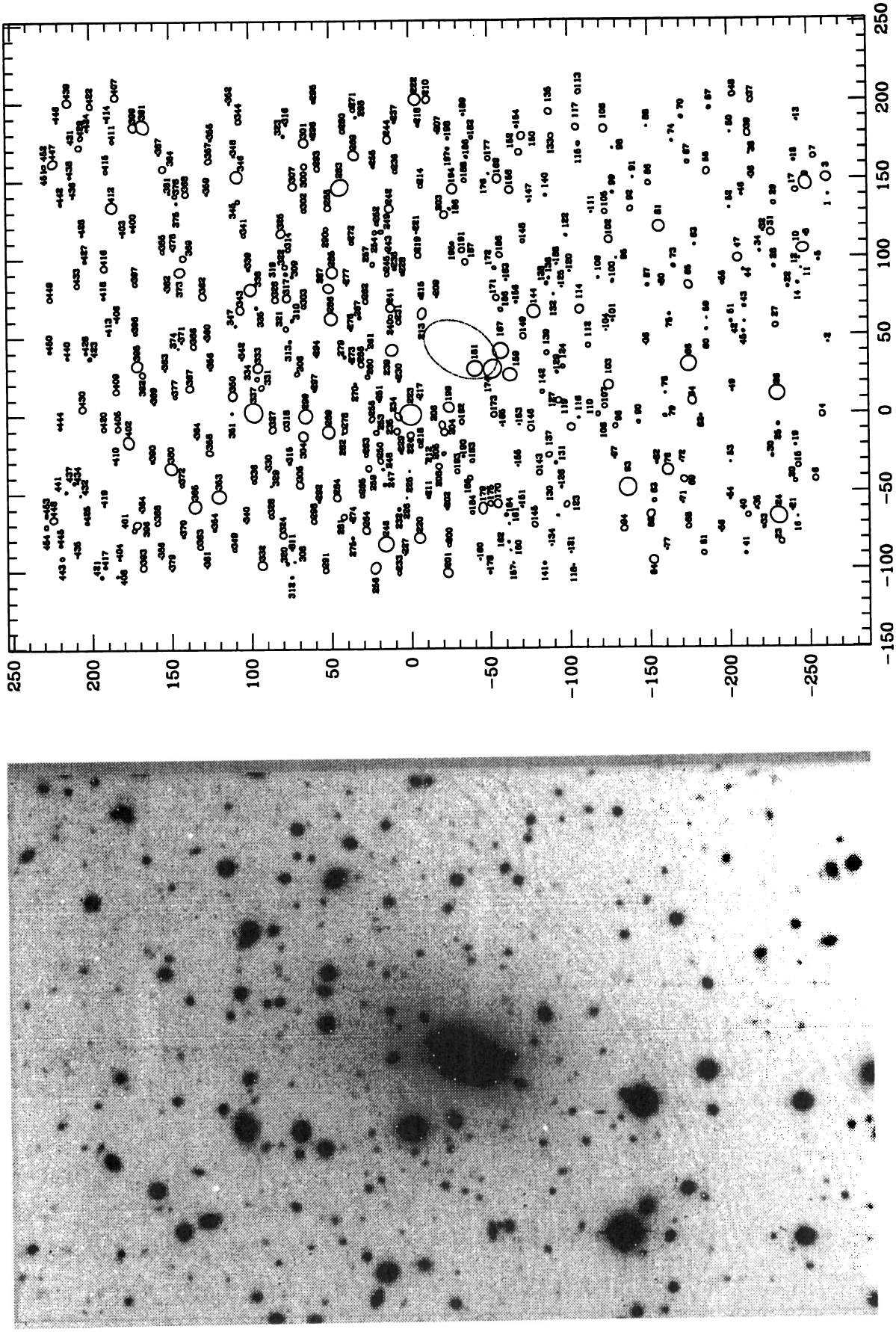

Fig. 4. a) An r-band picture of A3284. North is up, east to the right. b) Cross-identification chart for the field of the cluster (few bright stars saturated are not included). Numbers are entries in Table 3. Coordinates are in pixels (1 px = 0.675 arcsec) with respect to the centre of the cluster. The central cD galaxy is displayed as a dotted ellipse about $(X, Y) = (42, -32)$

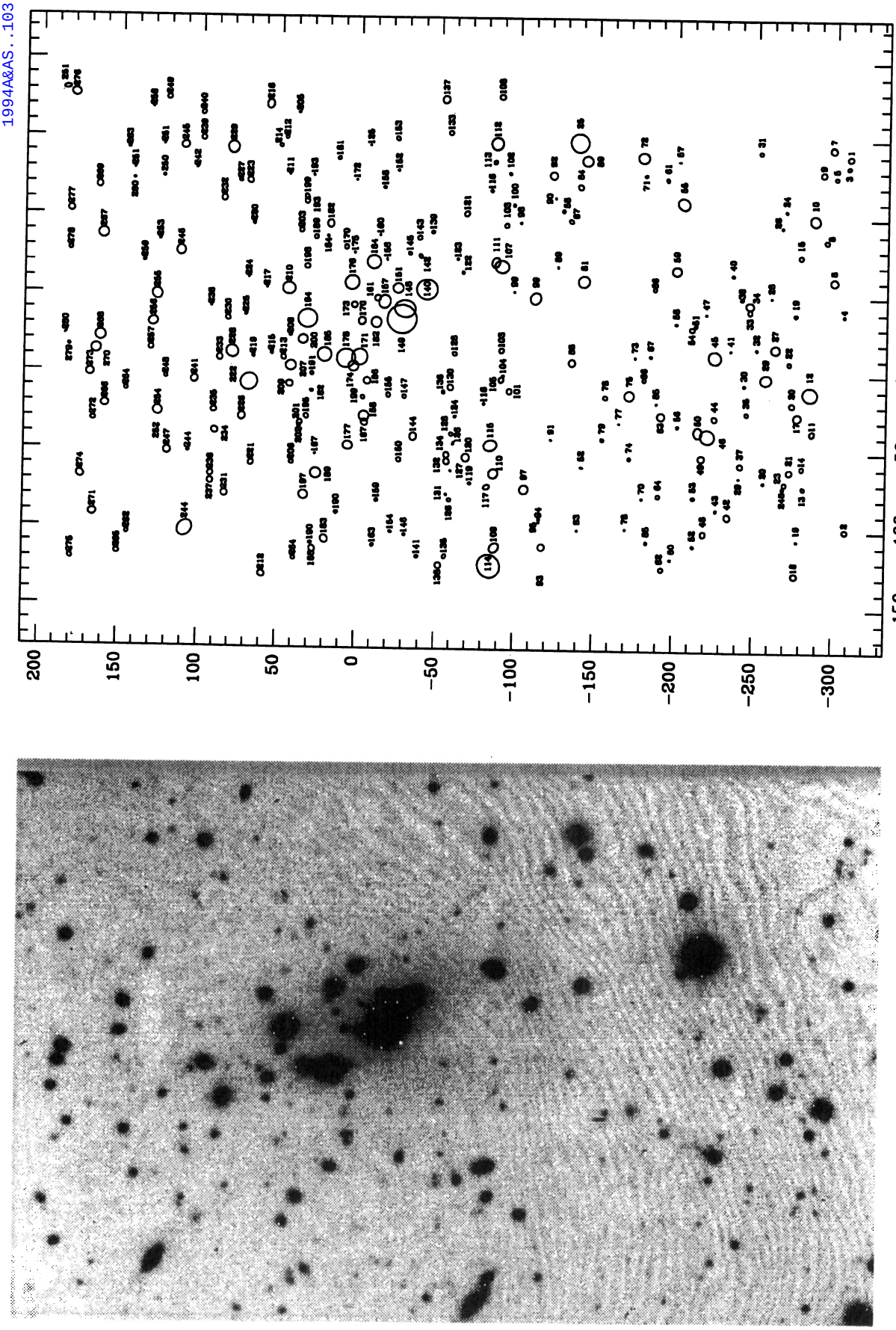

Fig. 5a,b. Same as Fig. 4a,b but for A3305. Numbers in panel b) are entries in Table 4

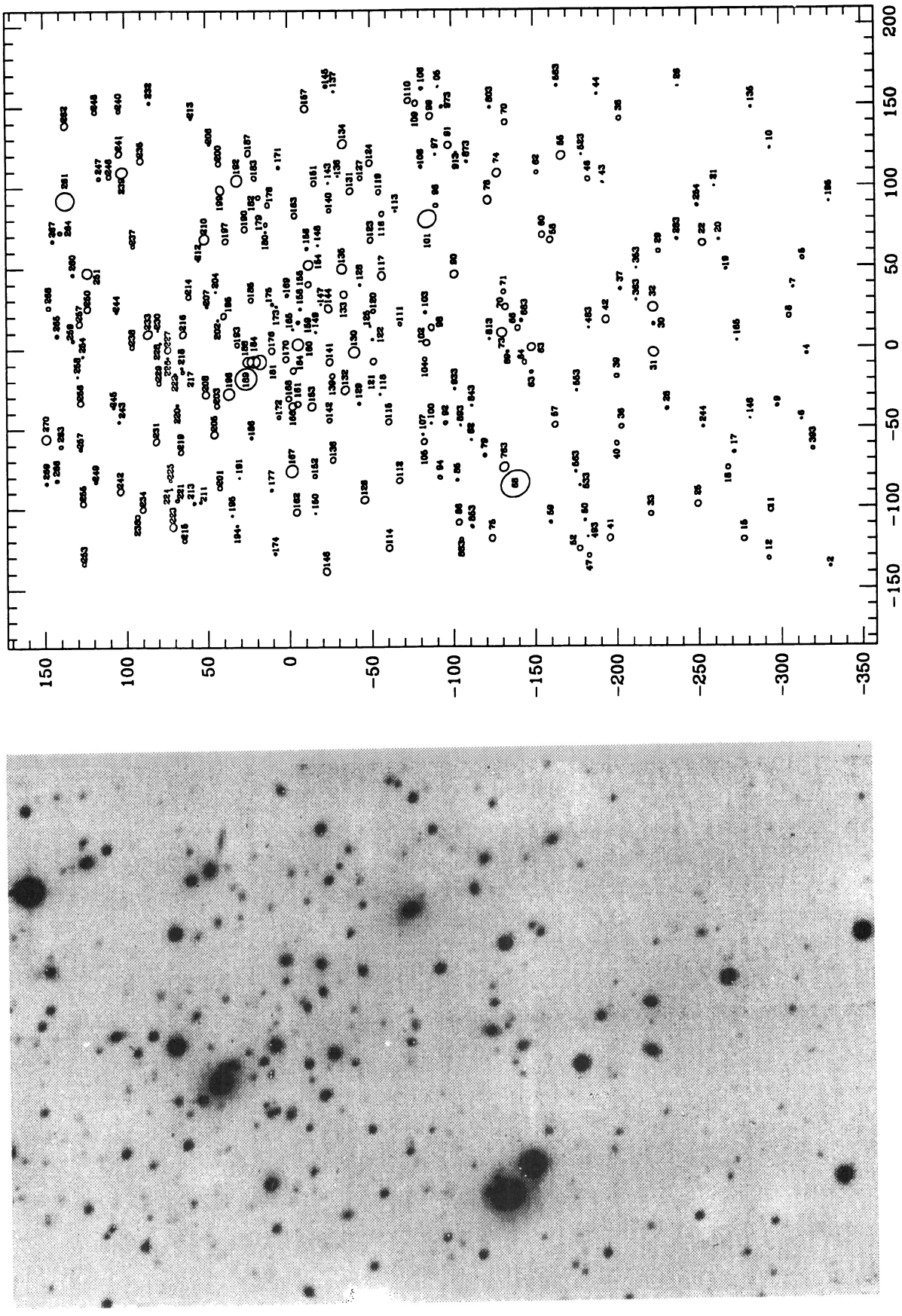

Fig. 6a,b. Same as Fig. 4a,b but for A1942. Numbers in panel b) are entries in Table 5

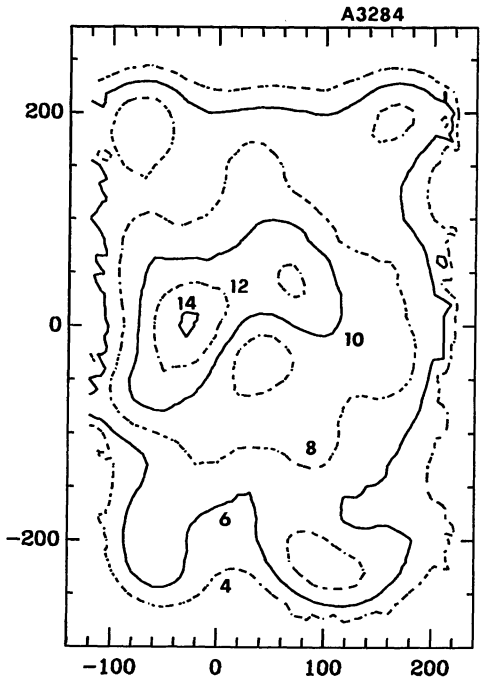

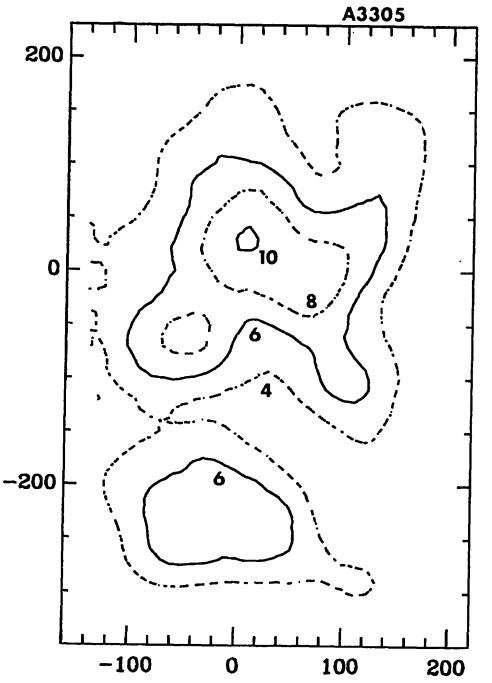

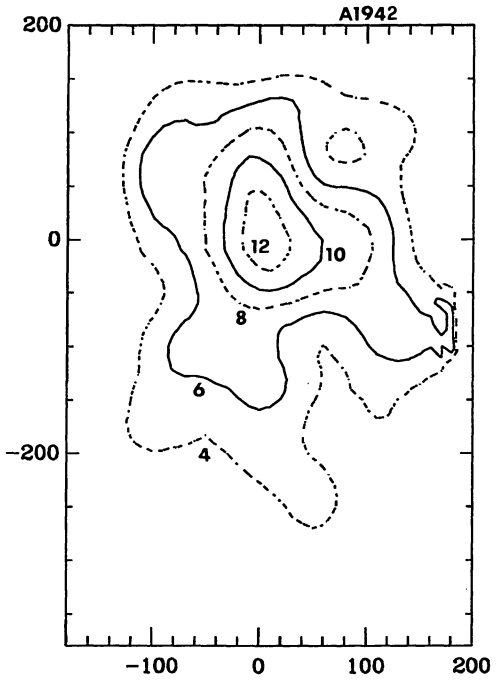

Fig. 7a,b,c. Contour levels of the object density in the three clusters from Tables 3-5. Labels are in unit of 10^4 objects/deg^2

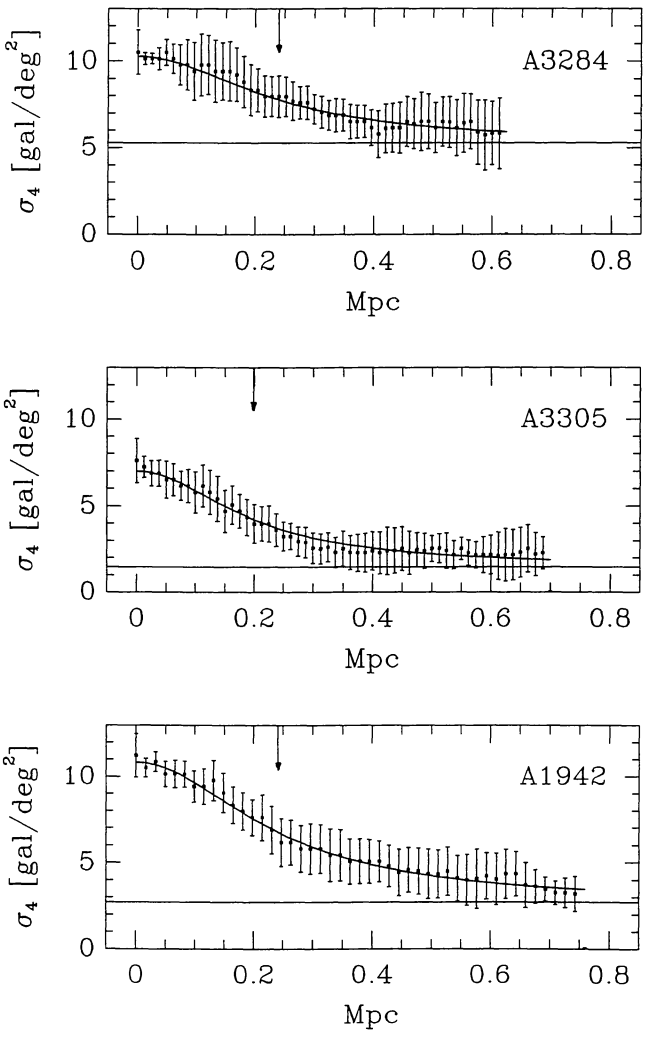

Fig. 8a,b,c. Comparison between the observed count density of the r sample in the clusters and the fitting King profile. The different levels of the background are displayed in each panel by the horizontal solid lines while the vertical arrows indicate the core radius. Error bars in the observations are at 1-σ level. Surface density σ_4 in the counts is given in unit of 10^4 obj/deg^2

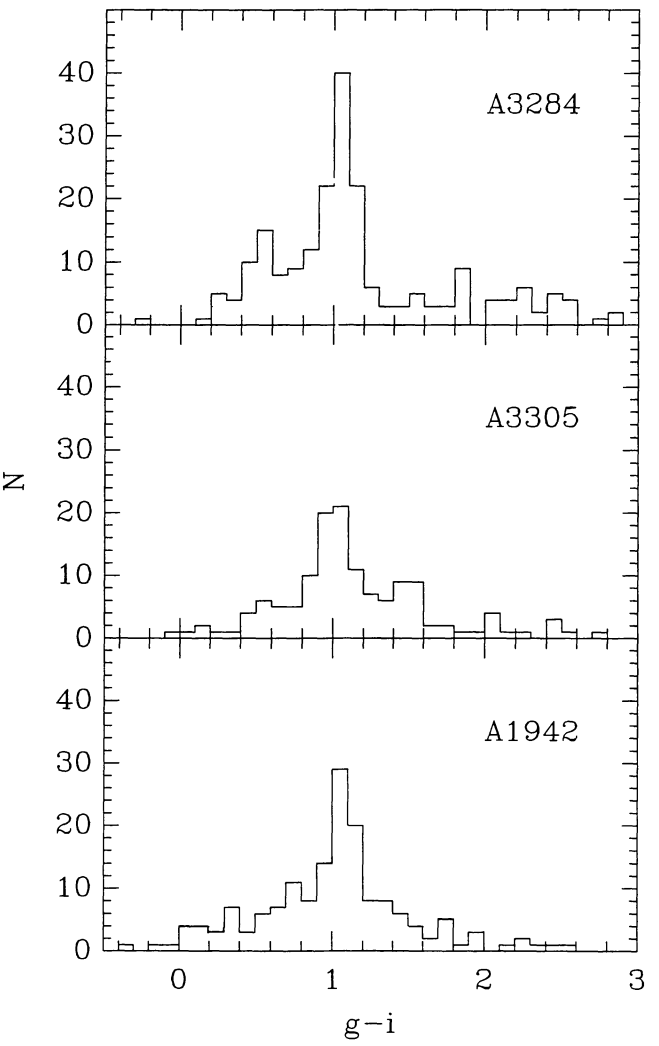

Fig. 9. Colour distribution in $g-i$ for the objects in the catalogs of the three clusters. A total of 209 objects are available for A3284, 136 objects for A3305, and 163 objects for A1942. Note in each histogram the big red peak about $g-i \sim 1$ attributed to early-type galaxies, and the smaller bump to bluer colours for the spiral galaxies. See text for discussion

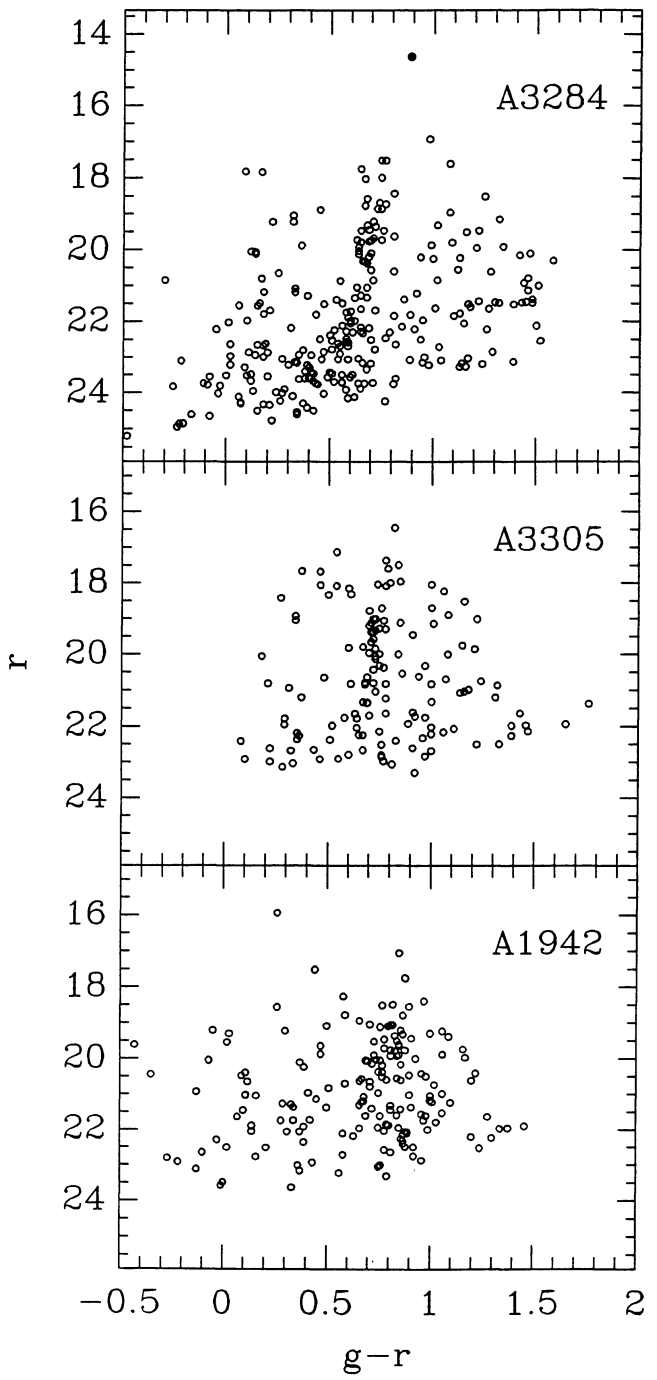

Fig. 10. Colour-magnitude diagrams for the three clusters. It is evident in each panel a vertical strip about $g - r \sim 0.7$ populated by early-type galaxies. The Visvanathan-Sandage (1977) c–m effect appears with the brightest ellipticals to be also the reddest ones. Note that the location of the central cD in A3284 in the diagram [the filled dot in panel (a)] is consistent with the effect

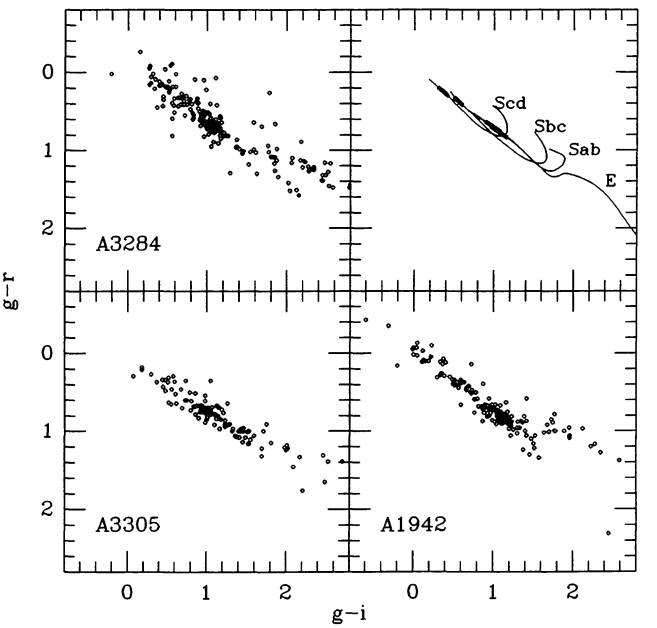

Fig. 11. Two-colour $(g-r)/(g-i)$ diagrams for the complete photometry in the fields of the three clusters. Upper right panel shows the expected loci with increasing redshift from $z = 0 \rightarrow 1$ (in the sense of increasing $g - i$) for elliptical galaxies (E) and spirals of different types (Sab, Sbc, Scd). Boldface mark the expected colours in the range $0.15 < z < 0.22$